DEPARTMENT OF PHYSICS

UNIVERSITY OF JYVÄSKYLÄ

CHARACTERIZATION OF A NEW PLASTIC SCINTILLATION MATERIAL AND COMPARISON WITH LIQUID BC-501A SCINTILLATOR

BY

OLEKSII POLESHCHUK

Master's thesis

Supervisor: Heikki Penttilä

Jyväskylä, Finland

2015

Abstract

In this work the capability of various scintillation materials to discriminate gamma rays and neutrons were studied. Also such basic properties of scintillators as light emission spectrum and light output were determined. The studied materials were BC-501A liquid scintillator and a plastic scintillator provided by CEA. An experimental setup consisting of detector shielding, analog and digital electronics and data acquisition system was built to study the neutron-gamma discrimination properties of the scintillation materials.

Pulse shape discrimination (PSD) technique was utilized. A computer code with a PSD algorithm was written. This code integrates the scintillation pulse waveforms over suitable time ranges for discrimination. Radioactive sources of Na-22, Co-60 and Cs-137 were used to examine the light output from the scintillation material. The neutron-gamma discrimination properties were studied with Cf-252 source. Liquid scintillator shows better discrimination capability than the studied plastic detector.

Contents

List of Figures

List of Tables

Introduction

Nowadays a wide range of scintillation materials are used in various fields of medicine and security as well as scientific purposes in research institutions. Depending on the field of application, the purpose of use can be medical imaging, ionizing radiation detection or spectroscopy, to mention a few.

Scintillation materials can be made out either of organic or inorganic materials and solvents. Gaseous materials can be used for scintillation counting. The most common example of this is the use of ^{3}He counters for neutron detection [36]. Most commonly, the scintillator materials are liquids, plastics or crystals. The scintillation light production mechanism of liquids and plastics is different from that of scintillation crystals. In crystals, the lattice structure has an important role in the scintillation mechanism. In the liquids and plastics, the light is emitted by single molecules.

Liquid scintillators are well studied and widely used. This type of scintillators shows good energy resolution and detection efficiency. Their major disadvantages are flammability and toxicity of solvents. The scintillating structures are aromatic carbohydrates that are considered to be carcinogenic. The containers for liquid scintillators are often at least partially made of fragile materials such as glass and quartz.

Plastic scintillators are more durable and can be machined almost to any shape. However, capability to discriminate neutrons and gamma rays is not typically associated to plastic detectors. Only recently there has been increased interest to develop discriminating plastic materials. In this work an experimental plastic detector developed and synthetized by CEA, France, was tested for pulse shape discrimination properties and its properties were compared to BC-501A liquid scintillation material with known neutron discrimination capabilities.

1. Basics of scintillation materials and scintillation light amplification

Conversion of ionizing radiation into light became possible with the advent of scintillation materials. The first device based on scintillation materials has been built by Crookes [1] at the beginning of the 20th century. Development and construction of one of the first organic scintillation detectors in the 1940's has been described in [2 – 4].

Nowadays ionizing radiation to light conversion process takes place in the numerous detection units in experimental nuclear facilities all over the world. Scintillators based on organic materials are widely used. Examples of application of organic scintillators could be found in already existing facilities or setups under construction, such as NOνA, USA [5] and LENA, Finland [6] for neutrino detection and in DEMON, France [7] for neutron detection.

Some types of scintillators allow not only detect the presence and energy of ionizing radiation but also determine the type of ionizing particles. Such a technique was used in this work to discriminate between neutrons and gamma rays.

For radiation detection, scintillation light from the detectors has to be converted into electrical signals. This conversion is done by photo sensors. The electrical signals generated by photo sensor can be received and analyzed either by analog or digital acquisition systems.

In this work a photomultiplier tube (PMT) was used for scintillation light detection. Therefore, in the second part of introduction the basics of PMT operation will be described.

1.1.Organic scintillators

The scintillation of organic materials is associated to molecular structure known as π-bond. The typical example of π-bond or π -electrons structure is formation of a benzene molecule, shown in Fig. 1.1 [8, 9]. This kind of structures form an excitation state spectrum schematically shown in Fig. 1.2. The singlet states are electron excitations where the electron spins are coupled to 0. Each of these states has a band of vibrational states build on them. Even the lowest vibrational state has a relatively high energy of the order of 0.1 eV, which cannot be thermally excited in the normal room temperatures [9, p.224].

Upon the absorption of energy in the molecule, only the singlet states (S = 0) are excited. The states above the S_{10} state decay in picoseconds to S_{10} state. The S_{10} state decays to the vibrational states of S_0 ground state with a time constant corresponding to a few nanosecond lifetime of emitting photons. These photons represent the so called prompt component of the scintillation light.

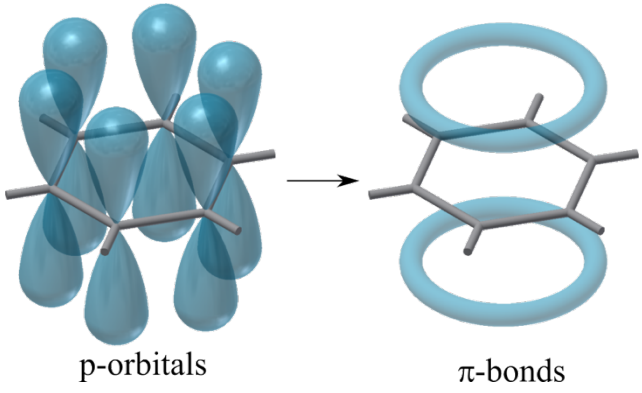

Fig. 1.1 Formation of π-bonds in benzene molecule.

The S_{10} state can also be converted to a T_1 triplet state via so called intersystem crossing transition. The T_1 state has up to million times longer lifetime than the S_1 state. The decay of the T_1 state to the S_0 ground state is so slow that the photons from it do not contribute to the scintillation light. Besides, as seen from Fig. 1.2, the wavelength of this light is different of that of prompt scintillation from S_1 state. However, molecules on T_1 state can be excited via absorption of thermal energy back to S_1 state in a much faster time scale. Photon emitted in the decay of this regained S_1 state is then contributing in the scintillation light pulse as the so called slow component. [8]

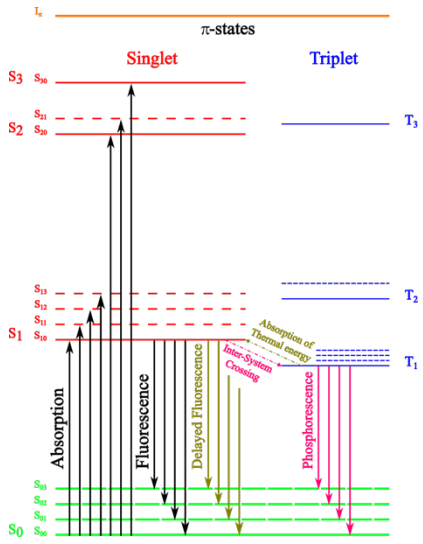

Fig. 1.2 States of an organic molecule raised from π-electron structure. Singlet S_x states and triplet T_x states are represented by solid lines. Corresponding S_{xx} and T_{xx} vibrational states are represented by dashed lines [from 10, p. 47].

Energy transfer to the scintillation material

Transfer of gamma ray energy to scintillation materials can be described by one of the three fundamental types of interaction of electromagnetic radiation with matter: Compton effect,

photo-electron effect or pair production. All these processes are fundamentally inelastic collisions of photon with the scintillation material. In the Compton effect a gamma ray interacting with an electron partially transfers its energy to the electron. Then a gamma ray with the reduced energy deviates from the initial trajectory at some angle θ. The kinetic energy of the Compton electron is the energy difference of the initial and scattered gamma rays.

The energy of the photon after interaction is:

$$E_{\gamma 2} = \frac{E_{\gamma 1}}{1+\frac{E_{\gamma 1}}{m_e c^2}(1-cos\theta)} \quad (1.1)$$

where $E_{\gamma 1}$ is the energy of the incident photon, $E_{\gamma 2}$ is the energy of the scattered photon, $m_e c^2$ is rest mass energy of the electron.

The kinetic energy of the recoil electron is:

$$E_e = E_{\gamma 1} - E_{\gamma 2} \quad (1.2)$$

The total energy absorption of gamma ray by an atom is called photo-electron effect. In this effect gamma ray totally transfer its energy to a K or L shell electron. The electron emitted from the atom in this interaction is called photoelectron. The energy of the photoelectron is:

$$E_e = h\nu - E_b \quad (1.4)$$

The last type of interaction is pair production. In this process the gamma photon is converted to an electron-positron pair via interaction with the electromagnetic field of the nucleus of the atom. This interaction can happen if energy of an incident gamma exceeds 1,02 MeV, the rest mass energy of an electron-positron pair. The total kinetic energy of the electron – positron pair is equal to:

$$E_{ep} = h\nu - 1{,}02\ MeV \quad (1.5)$$

Neutrons interacting with atoms can be scattered or absorbed only by the nuclei of the atoms. The most widely used method of fast neutrons detection is elastic scattering of neutrons by light nuclei. In the scattering process a neutron transfers a part of its energy to the scattering light nuclei. The recoiling ions then transfer their kinetic energy to detector material in atomic collisions. The best neutron scatterer material is hydrogen, since in principle a neutron can transfer all its kinetic energy to a hydrogen nucleus (proton) in a single head-on collision.

Slow component of the scintillation light

Gamma ray absorption in a scintillation material of a detector always leads to the production of electrons. Collisions of these electrons are then finally depositing energy to the detector. In neutron interaction a heavy ion is generated. The energy deposition to the detector in this case is different. The difference in *linear energy transfer* (LET) dE/dl between gamma ray and neuron in detection material cause the difference in the slow components of signals generated by these types of radiation. This effect is used for pulse shape discrimination [10, p. 221].

The scintillation light emitted after energy absorption is converted to the electrical signals. An example of a signal obtained from an organic scintillator is presented in Fig. 6.3. A comparison signals after neutron and gamma ray absorption in the detector obtained from two different organic scintillators are shown in Fig. 6.1 and Fig. 6.2. These signals contain a fast rise component and a slow decay component. The rise time of the signals remains unchanged for all types of radiation. However, the decay time of the slow component (Tail integrals in Fig. 6.1 – 6.2) varies depending on the nature of interacting particle.

In [10, p. 233], Birks compares three theories, which describe the nature of the differences in the slow components. Based on these theories Birks proposes a theory which more accurately describes the scintillation process in organic scintillators.

The decay time of the slow component according to the first theory depends on the time of ion recombination in the singlet states of an organic molecule. The second theory is based on excitation of the molecule to the higher triplet states. The decay time in this case is depends on the time of the triplet-singlet transitions and does not depend on the time of ions recombination in the triplet states. The third theory suggests that the slow component depends on interactions of *excitons*. An exciton is a pair of interacting neighbour molecules excited to higher energy states. Interaction between excitons forms excited states of the whole system. According to this theory the decay time of such states determines the decay time of the slow components.

The theory proposed by Birks combines some suggestions from each of the theories above. As in the third theory the slow component arises from interactions between excitons. However, exciton molecules in Birks's theory are excited to the triplet state T_1. The interaction between the excited pairs of molecules in this state leads to formation of two molecules one of which is in S_1 state and another is in S_0 state. In this case, the determining factor of the slow component is the decay time of the excited T_1 state.

1.2. Photomultiplier tubes

Photomultiplier tubes (PMT) are used for conversion of photons into electrons and further into detectable electrical signals. These devices are applied in fields where light detection is necessary and the amount of light must be quantitatively described. One of the main fields of application is scintillation detectors.

Typical PMT consists of input window, photocathode, input optics (focusing electrodes, accelerating electrodes), multiplier (dynodes) and anode. All these components are located in glass envelope under vacuum. This envelope is attached to the tube base, which is designed in accordance with connection standards like 14 pin JEDEC B14-38, 20 pin JEDEC B20-102, etc.

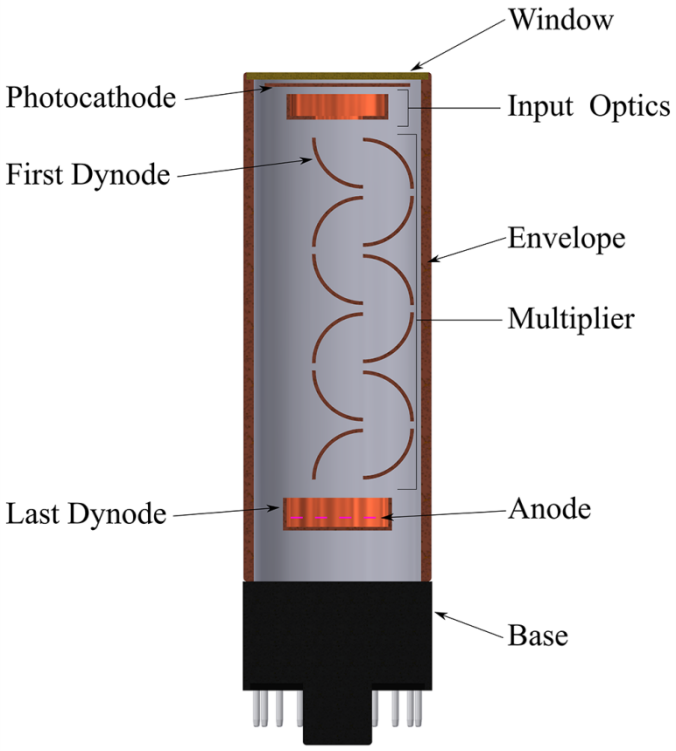

Fig. 1.3 Structure of a PMT.

Photomultiplier should be chosen in accordance with the properties of the light source and experimental requirements. Attenuation coefficient of the window material should be as low as possible for the wavelengths of the incoming light. Multiplication and time response of a PMT should meet the experimental requirements. The conversion efficiency from photons to electrons is described by parameters called *quantum efficiency* or *radiant sensitivity*. The photocathode should have the highest quantum efficiency or radiant sensitivity for the light spectrum in case of the pulsed light or light flux correspondingly [11, p.37]. Quantum efficiency is ratio between the number of photoelectrons emitted from a photocathode and amount of incident photons. Radiant

sensitivity is a term which is applicable only to photon fluxes. This parameter describes the dependence between the photon flux and the photoelectric emission current [12].

Photocathode and photoelectric effect

One of the two fundamental effects which lie behind the operation of a PMT is photoelectric effect. This effect takes place in photocathode and is responsible of electron emission from the cathode surface due to interaction with photons. Photoelectric effect is characteristic of so called photoemissive materials from which the cathode is made. Alkali halide (Sb-Cs, etc.), Bialkali (Sb-K-Cs, Sb-Na-Cs, Sb-Rb-Cs, etc.), Multialcali (Sb-Na-K-Cs, etc.), III-V compound semiconductor materials are among others widely used photoemmisive materials for cathodes production. Each of these materials has high sensitivity only in single narrow spectral region. Comparison of the characteristics of the most common photocathode materials are presented in Table 1.1. Terms Super Bialkali and Ultra Bialkali are adopted from reference [35]. Difference in the photocathode material properties emphasize the importance of correct selection a photomultiplier for a specific experimental goal.

In the photoelectric effect light interacts with cathode and transfer its energy to a cathode's electrons. Initially electrons in semiconductor materials are located in the valence band. Absorbing the photon, electrons become excited. The excited electrons move through the material and can reach the surface of the cathode. If the excitation energy of the electron at the surface is large enough to overcome the potential barrier at the material surface electron can be emitted from the cathode surface into vacuum. This process of electron emission is called photoelectric effect.

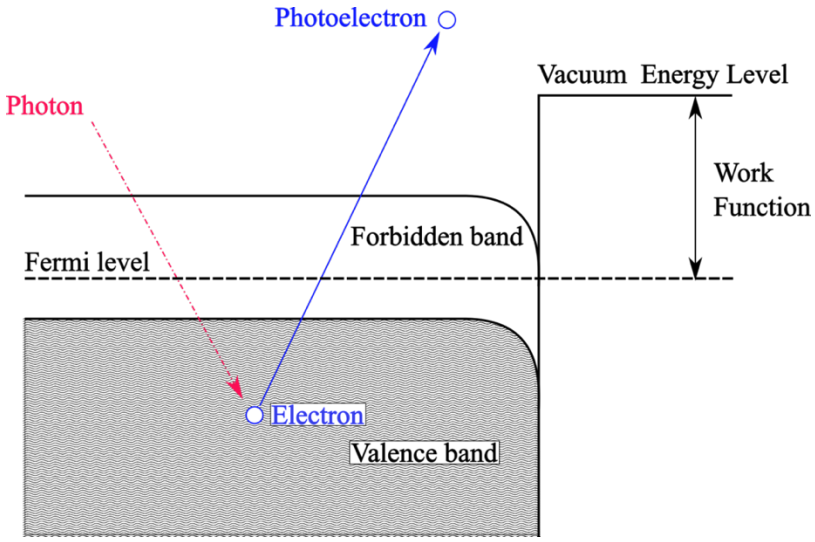

Fig. 1.4 Band structures of p-type semiconductor materials [from 13, p. 14].

A diagram of the band structure of semiconductors and the process of photoelectric effect in semiconductors is shown in Fig. 1.4. The band structure shown in this figure is that of a p-type semiconductor, in which a positive surface charge is created on the semiconductor surface. This charge forces the valence band and the forbidden band to curve down as it shown in the Fig. 1.4. This curvature leads to reducing of electron affinity. Thereby even a photon with energy lower than threshold energy could hit out electrons from a p-type semiconductor. [37]

Table 1.1 Characteristics of photocathodes spectral response. Data from [11, p.1-4], [13, p.33, p.35], [14, p.16] and [35].

Photocathode material	Sensitive range, nm	Wavelength of maximum sensitivity λ_{max}, nm	Quantum efficiency at λ_{max}, %	The maximum of radiant sensitivity, mA/W
Cs-I	115 – 200	130	13	14
Cs-Te	150 – 340	235	10	20
Bialkali	275 – 650	380	27	88
Super Bialkali	275 – 650	350	35	–
Ultra Bialkali	275 – 650	350	43	–
Multialkali	160 – 850	420	25	64

Dynode and Secondary emission

Another important fundamental process of a PMT operation is secondary emission from dynode electrons. The electron multiplication in a PMT can be described through this process.

The electrons created by photoemission are accelerated and directed towards the first dynode. Before hitting a dynode, accelerated electrons reach an energy that is sufficient to release on the average more than one electron from the dynode. The amount of released electrons is proportional to the electron energy. Release of secondary electrons can be described in the same way as the release of photoelectrons. [9, p.280; 13, p.17]

The typical structure of a dynode is shown in Fig. 1.5. The dynode surface towards the beam of accelerated electrons is coated by a thin layer of material which easily emits electrons.

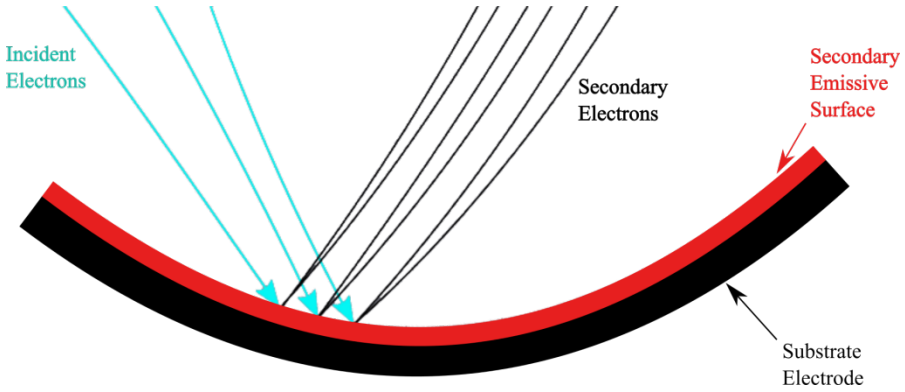

Fig. 1.5 Dynode structure.

A PMT includes several dynodes as shown in the Fig. 1.3. Dynodes in a PMT form so called cascade structure. This cascade structure significantly increases the current of electrons. The geometry and the surface material of the dynodes influence on the PMT performance. Variation of these allows manipulation of e.g. the time response and gain of a photomultiplier tube.

At the last step an electron avalanche created in the multiplication stage is directed to an anode. The main purpose of the anode is efficient collection of these electrons. The collected electrons in the anode create the anode current from which the output signal is generated. [13, p.18; 14, p.4]

Except photomultipliers, such devices as conventional photodiodes, avalanche photodiodes and silicon photomultipliers (SiPM) can be used as photon detectors for scintillation light detection. These devices have some advantages in comparison with PMTs. Photodiodes can be applied in magnetic fields. They have higher quantum efficiency. On the other hand, their spectral response does not properly match to the scintillation wavelengths of neutron-gamma disrciminating materials. The dark current is much higher than that of photomultiplier tubes. This has limited the use of solid state devices instead of traditional photomultiplier tubes in pulse shape discrimination applications. Nevertheless, in [15] the potential use of SiPM detectors with organic crystal and plastic scintillators for neutron – gamma discrimination was shown.

2. Comparison of scintillation materials: the experimental setup

The studies of the discrimination properties of the scintillation materials benefits significantly on proper shielding of the detector setup from the background radiation. This shielding was built in a way to allow fast access to the detector system and radioactive sources. The scintillation light emission pulses were amplified with fast response photomultiplier tube and recorded with a fast waveform digitizer. The pulse shapes were stored on computer hard disc and analyzed off-line.

The light to photon conversion and electric signal amplification assembly consisted of Hamamatsu head-on R1828-01 photomultiplier tube [16] connected to Ortec 269 photomultiplier base [17]. NHQ 204M high voltage power supply was used to fed Ortec 269. This assembly produces analog, electric signals from scintillation light output.

Data was acquired with two systems. In the analog acquisition, the photomultiplier anode signals were connected to Ortec 113 preamplifier, which is specifically designed for scintillation counting. This setup allows measuring the energy spectra using spectroscopy amplifier Ortec 471 for shaping the preamplifier signal and providing it to a pulse height sensing analog-to-digital converter (ADC). The preamplifier however regenerates the signal and stores only the energy information. More specifically, the preamplifier collects the charge from the anode and provides a voltage signal. The height of the signal is proportional to the collected charge. The shape of the voltage signal depends only on the electronic components of the preamplifier, and information of the original scintillation pulse shape is lost.

There are hardwired analog electronic modules designed for pulse shape analysis, such as NDE 202 [18]. Since very little was known about the properties of studied scintillators, more flexible approach was taken. The signal from the anode was directly connected to a digital data acquisition system, consisting of Caen N6751 digitizer [19] and custom acquisition software [Jaakko Julin, Accelerator based material physics group, Jyväskylä] running on a Linux-powered computer. The waveform was stored with resolution of 0,5 ns/channel. Each signal contained 602 time channels. This way the original signal shape was not distorted and pulse shape analysis could be applied.

A photomultiplier can give relatively high instantaneous current which in principle can damage the digitizer. In the progress of the experiments, a fast amplifier Phillips Scientific model 775 with low amplification therefore was tried to be used between the photomultiplier anode and the digitizer. Fast amplifier repeats the shape of the original signal so it will not be distorted. Another purpose of this arrangement was to enhance the signal and improve the signal to noise

ratio. It turned out, however, that the setup works better without the fast amplifier, thus the fast amplifier is not shown in Fig. 2.1 and 2.4.

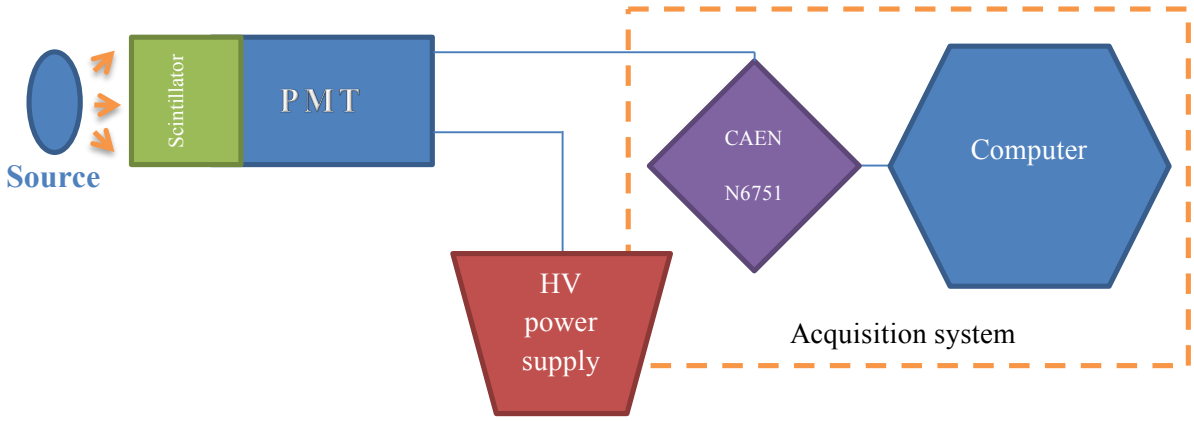

Fig. 2.1 Block diagram of the setup.

In this work two scintillation materials were used. The main purpose of the work was to study the properties of the first one, a novel scintillation plastic that is not commercially available yet. The sample was a solid plastic transparent cylinder whose diameter was 54 mm and height was 25 mm. Second material was well known BC-501A liquid scintillator packed in custom made container to be able compare scintillation properties of plastic scintillator with liquid scintillator of the same dimensions. Both samples are shown in Fig. 2.2.

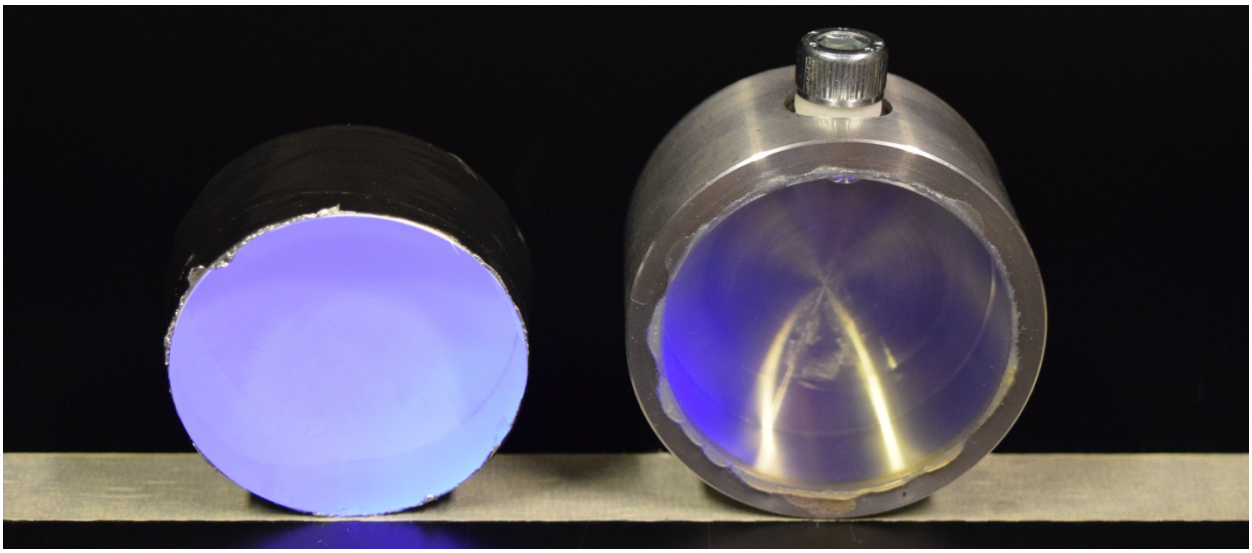

Fig. 2.2 Scintillation materials. The plastic scintillator sample is on the left and the liquid BC-501A scintillator in the cell used in the tests on the right.

To have the same volume of scintillation materials, a 50,5 mm inner diameter, 25 mm deep cylindrical container was built for the liquid scintillator (Fig. 2.3). The body of the cell was machined from aluminum rod. The walls were 5 mm thick. The top of the container was thinned to 3 mm, to allow low energy gamma rays to penetrate to the scintillation material. The bottom of the cell was sealed by quartz glass window that has wide optical transparency range (160 – 3500 nm). The quartz window was glued to aluminum cylinder with epoxy. After assembling of the container, it was filled with liquid scintillator BC-501A.

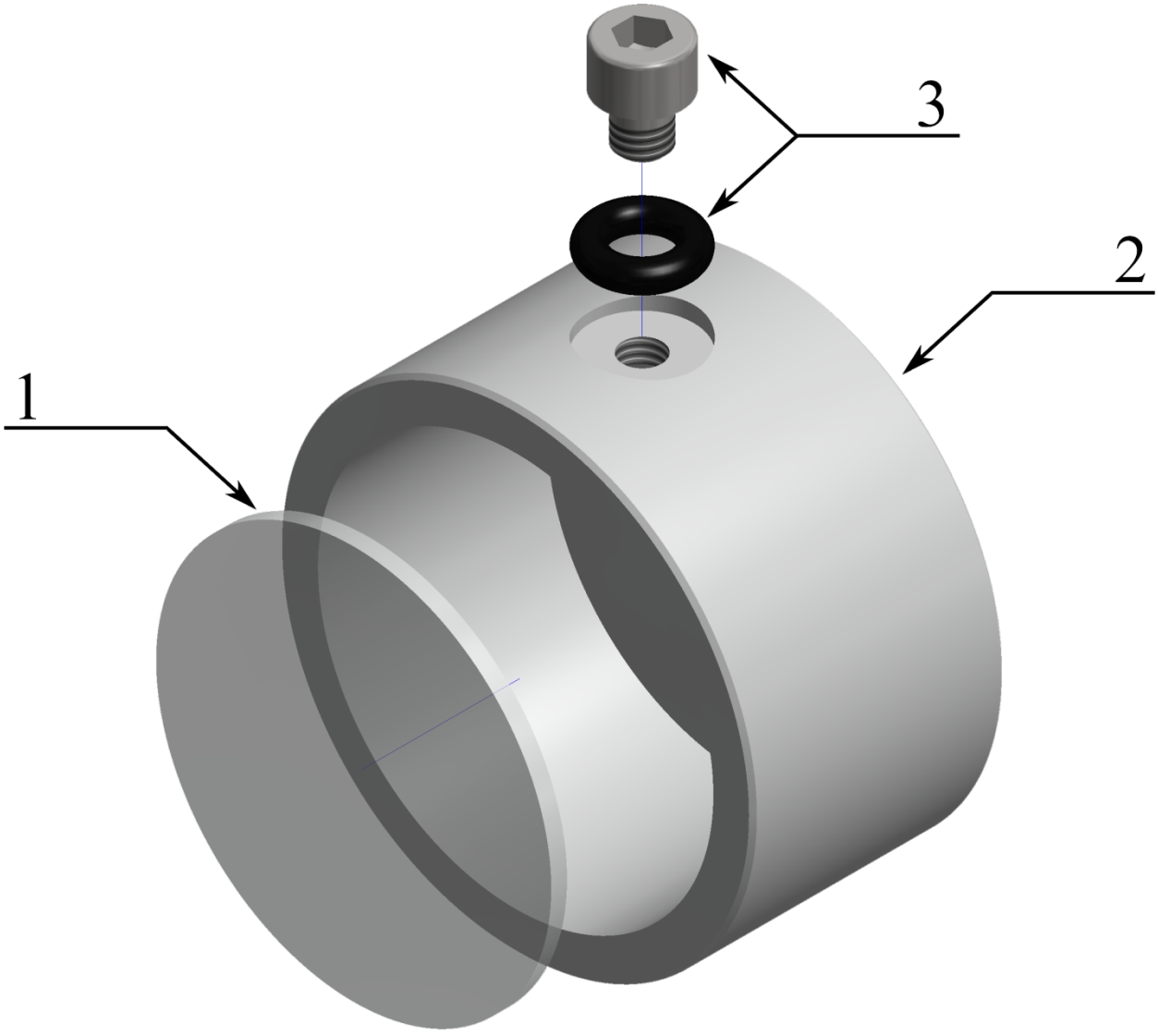

Fig. 2.3 Exploded view of the container designed for the liquid scintillator. 1 – Quartz window, 2 – Aluminum container, 3 – Sealing screw.

An important step of liquid scintillator preparations was deoxygenation with argon to remove the possible oxygen from the liquid, since the presence of oxygen in liquid scintillators reduces the light output. The scintillator samples were attached to PMT faceplate with Dow Corning Q2-3067 optical couplant. The plastic scintillator was also covered with black plastic tape to reduce the light generated background. The detector system (Fig. 2.5) including scintillator, PMT and PMT base were shielded with 50 mm thick lead blocks to decrease the influence of the background gamma and beta radiation.

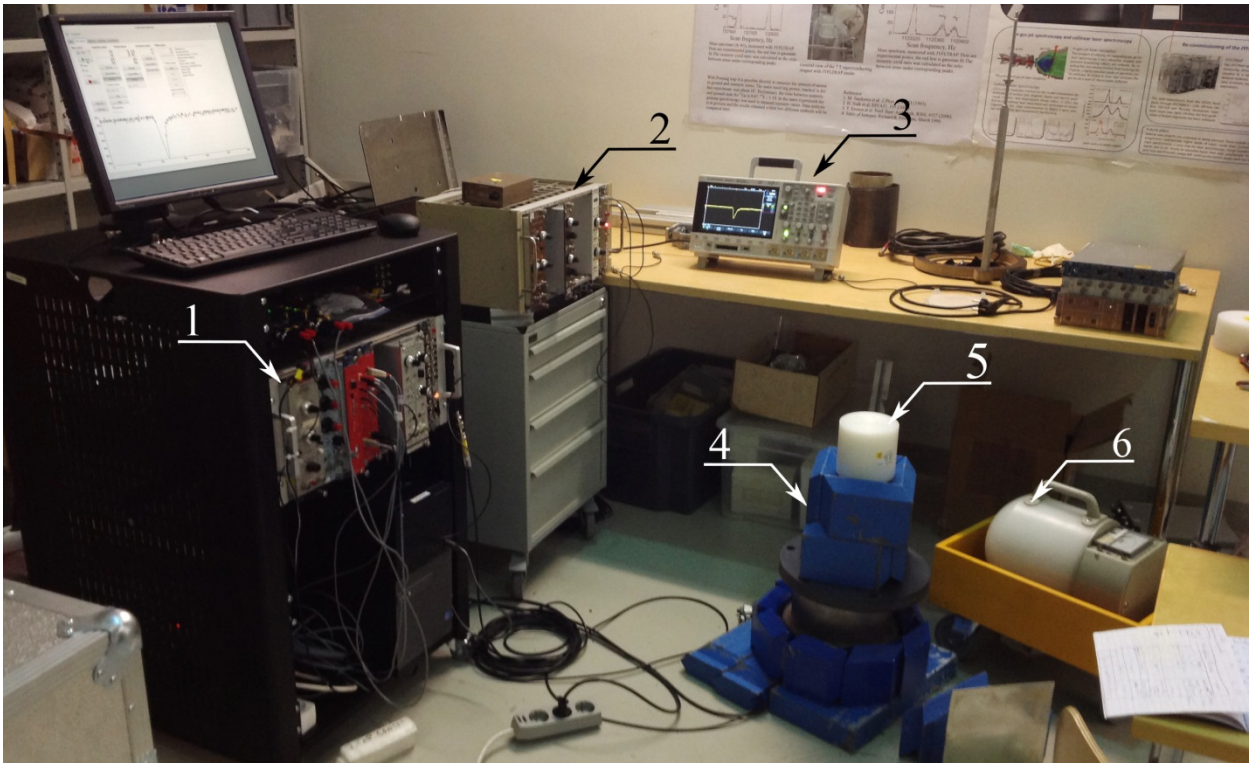

Fig. 2.4 Experimental setup. 1 – acquisition system including Caen N6751 digitizer, 2 – analog electronics and NHQ 204M power supply, 3 – Agilent technology DSO-X 3104A digital storage oscilloscope, 4 – detector shielded with lead, 5 – source, 6 – neutron dosimeter.

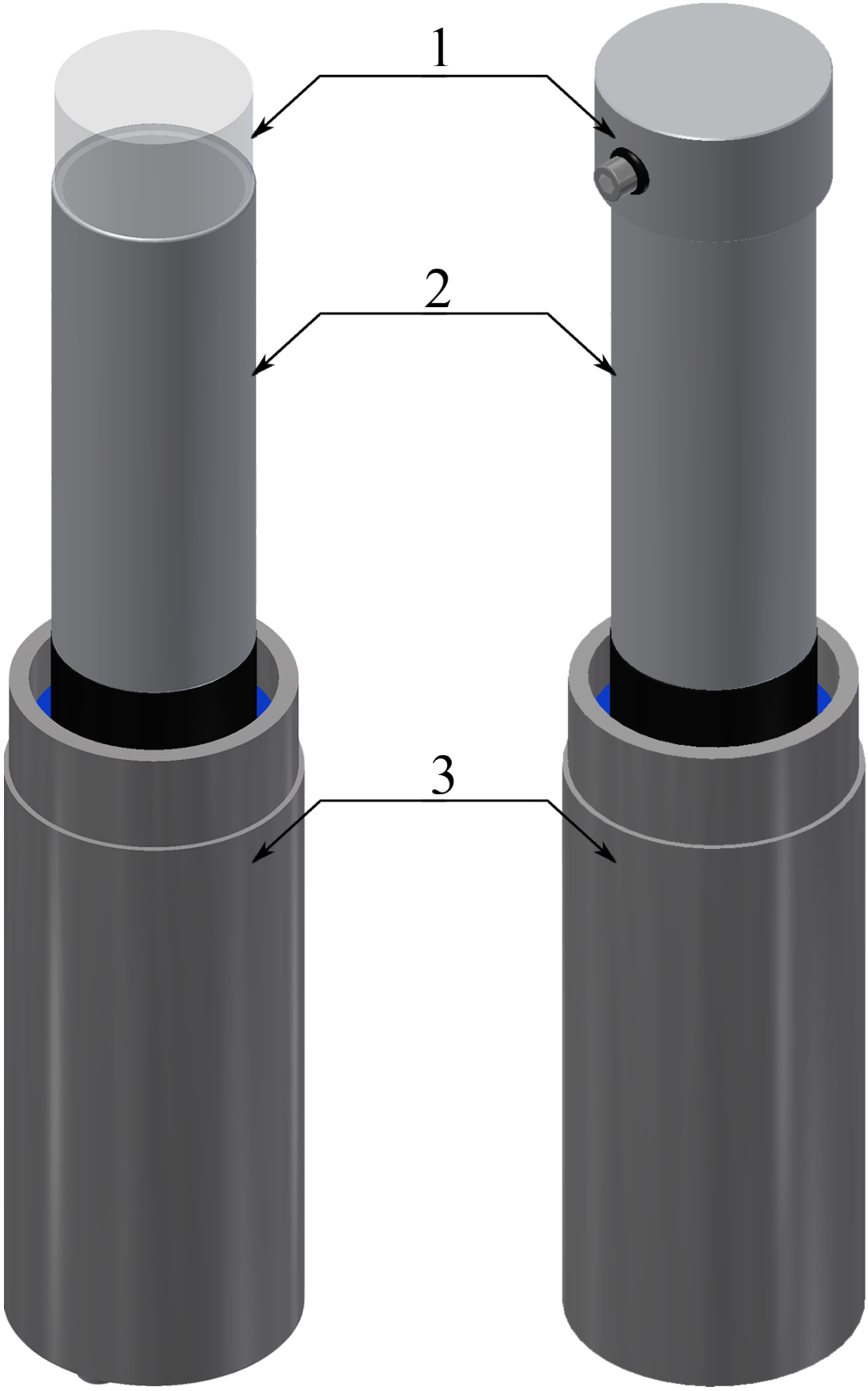

Fig. 2.5 Detectors. 1 – Scintillators, 2 – PMTs Hamamatsu R1828-01, 3 – PMT's bases.

Photo multiplier tube with scintillator was positioned vertically (Fig. 2.5). Radioactive source was placed 130 mm above the surface of scintillation material on a plastic support. It was centered with respect to the scintillators.

Measurements were made for each combination of scintillator and source with bias voltages in range -1300 – -1500 V. The purpose of the variation of voltage was to search for the optimal balance between the amplification and the scintillation pulse shape retention. PMT's anode was directly connected to the digitizer. Resolution of digitizer was 10 bit, sampling rate 2 GS/s and input range 1 Vpp. Typically, 100000 traces were stored for the off-line PSD analysis for each combination of radioactive source, scintillation material and bias voltage. If less events were used for the analysis in any case, the specific number of pulses is indicated near the calculations.

3. The scintillation light wavelength spectra

3.1. Experimental setup

It is important to know the scintillation light emission spectrum for the correct selection of a photomultiplier tube. One of the PMT selection criteria is matching between wavelength of maximum emission of scintillation material and the wavelength which corresponds to the maximum quantum efficiency of the PMT's photocathode.

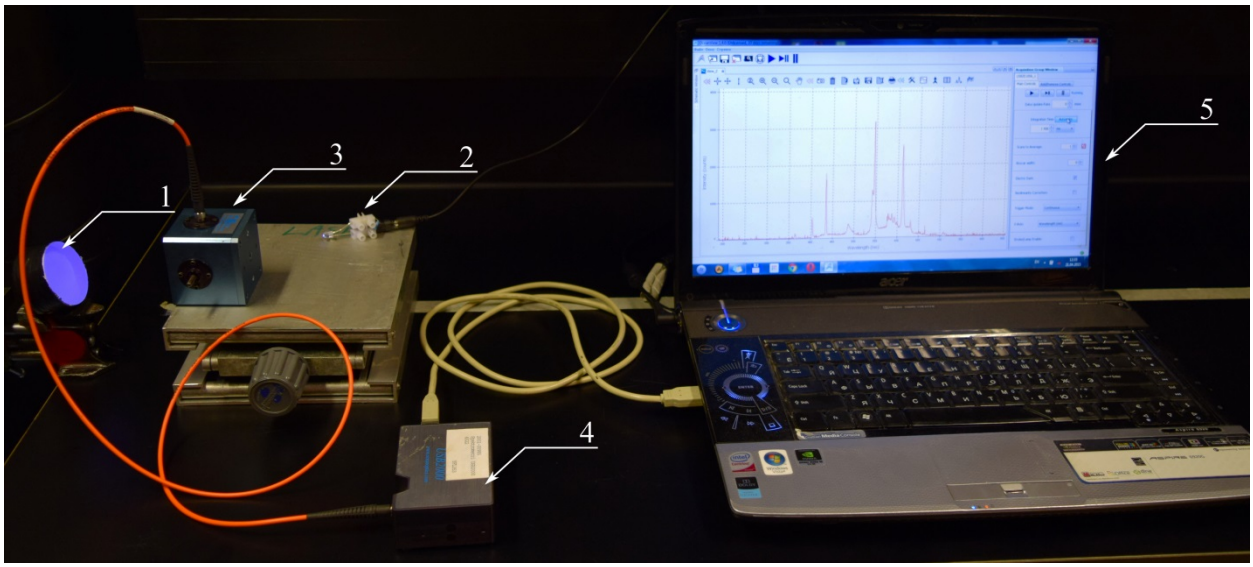

Fig. 3.1. Spectrometry setup for emission spectra measurements. 1 – scintillation material, 2 – LED 370nm, 3 – OceanOptics integrating sphere, 4 – OceanOptics USB2000 spectrometer, 5 – PC for data acquisition.

The emission spectra of the scintillation materials were measured with OceanOptics USB2000 spectrometer (Fig 3.1). The spectrometer was coupled with Thorlabs ∅200 μm, 0.22 numerical aperture (NA) optic fiber to OceanOptics integrating sphere. The integrating sphere was used as input optics to avoid any directional effects. The disadvantage of the sphere is large reduction of the input light intensity.

The most straightforward way to determine the scintillation light spectrum would have been to irradiate the scintillator material with a radioactive source and record the spectrum of scintillation light. It turned out, however, that the sensitivity of USB2000 was not high enough, not even without the integrating sphere. Therefore, a method similar to the one described in [20] was used. The studied scintillator material was exposed with a short wavelength LED. As discussed in chapter 1.1., the fluorescence light emitted by an organic scintillator material comes from the decay of S_{10} state. Thus, it does not matter, how the state is excited.

The scintillators were placed in front of entrance window of the integrating sphere and exposed by LED 370 nm (Fig. 3.4). Absorption of light in scintillation materials causes photoluminescence. This photoluminescence light was recorded with spectrometer.

Before measuring the emission spectra, the wavelength calibration of the USB2000 spectrometer was checked with a mercury lamp and intensity calibration with a NIST traceable quartz-tungsten-halogen calibration lamp. The comparison of reference and recorded data could be found in Fig. 3.2 and Fig. 3.3. Wavelength calibration showed a systematic error 0,44 ± 0,09 nm. Intensity calibration showed significant difference between calibration curve provided by manufacturer of the calibration lamp and the recorded data. After intensity calibration, calibration coefficients were found for each channel.

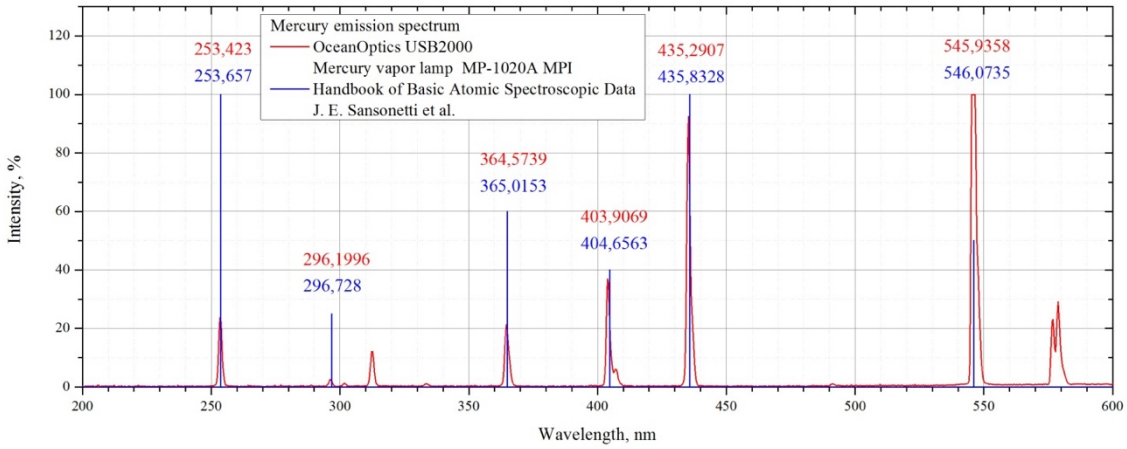

Fig. 3.2 Wavelength calibration of OceanOptics USB2000 spectrometer with mercury vapor lamp MP-1020A MPI.

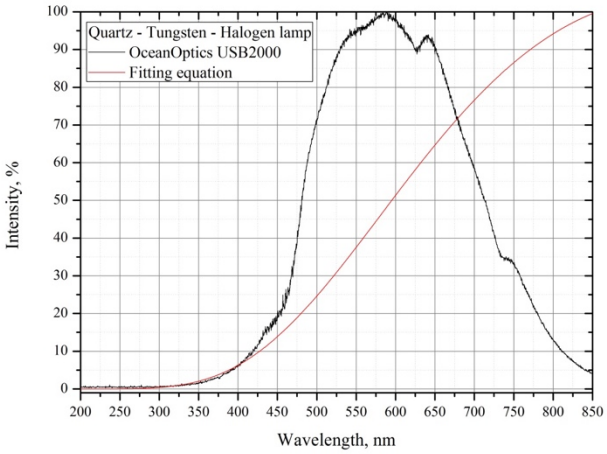

Fig. 3.3 Intensity calibration of OceanOptics USB2000 spectrometer with quartz-tungsten-halogen lamp.

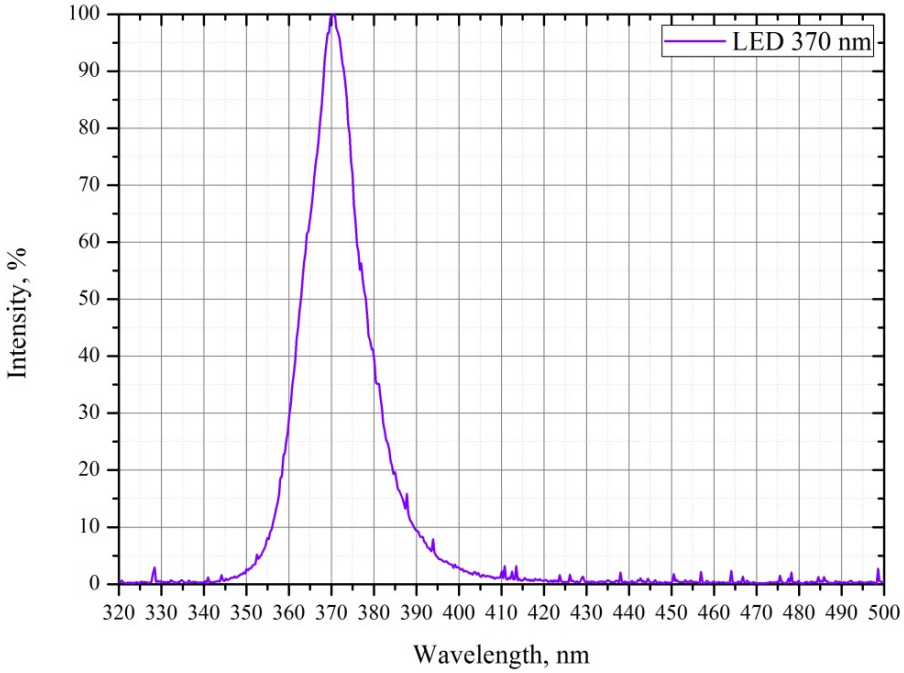

Fig. 3.4 Wavelength spectrum of the LED
used in scintillation emission spectra measurements (LED 370 nm).

3.2.Measurements and results

The method used for emission spectra measurements was similar to method described in [20]. The scintillation material samples were exposed with a LED. The LED was chosen in such a way that the wavelength of the LED was shorter than the wavelengths in the expected emission spectra of the scintillators. Fig. 3.5 shows typical emission spectra of BC-501A taken from [21]. Based on this spectra, was decided to use a LED with 370 nm wavelength.

There was no preceding knowledge of the emission spectrum of the plastic material. However, since it was expected to have similar properties as BC-501A, including gamma-neutron discrimination, its emission spectrum was supposed to be similar to that of BC-501A. The measured fluorescent light spectra in Fig. 3.6. and 3.4 support the assumption of the structural similarity.

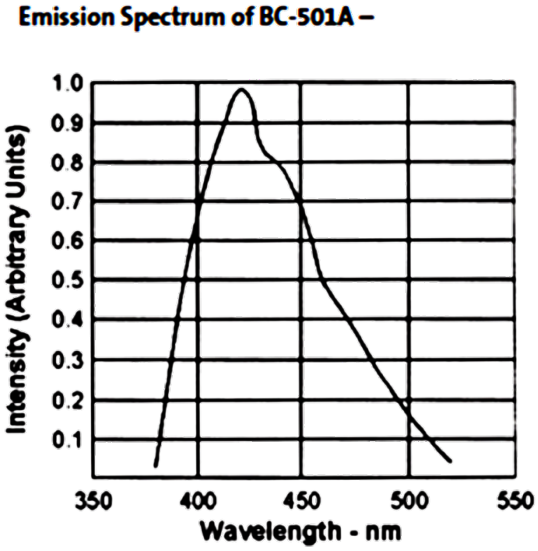

Fig. 3.5 Emission spectrum of BC-501A [from 21].

The initial recorded spectra (Black curves in Fig. 3.6 and Fig. 3.7) contain fluorescent light and scattered LED light. To retrieve emission spectra of scintillators (Blue curves), LED's spectra (Red curves) were subtracted.

The spectrum obtained with the liquid BC-501A scintillator Fig. 3.6 (Blue) has the same major features as the spectrum illustrated in the manufacturer's datasheet Fig. 3.5. The peaks at ~420, ~445 and ~475 nm are resolved more clearly in the current measurement. The small peak at ~395 nm is not observed as a resolved peak in the spectrum on the manufacturers data sheet. This can be due to insufficient resolution of the manufacturer measurement. However, since a similar peak at almost the same wavelength is seen in the emission spectrum of the plastic scintillator

(Fig. 3.7), a question arises whether they can be artefacts generated by the scattered light. Further investigations are needed to determine the nature of these peaks.

The wavelength of maximum emission, 420 and 429 nm for the liquid and the plastic scintillators correspondingly were obtained. The quantum efficiencies of the photocathode of the used Hamamatsu 1828-1 photomultiplier tube can be found in Fig. 4.8.

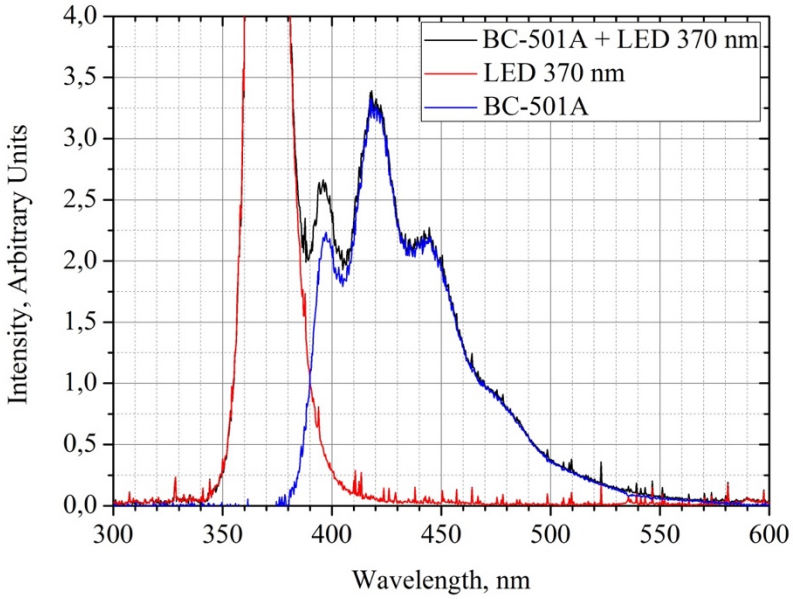

Fig. 3.6 Measured emission spectrum of BC-501A scintillator.

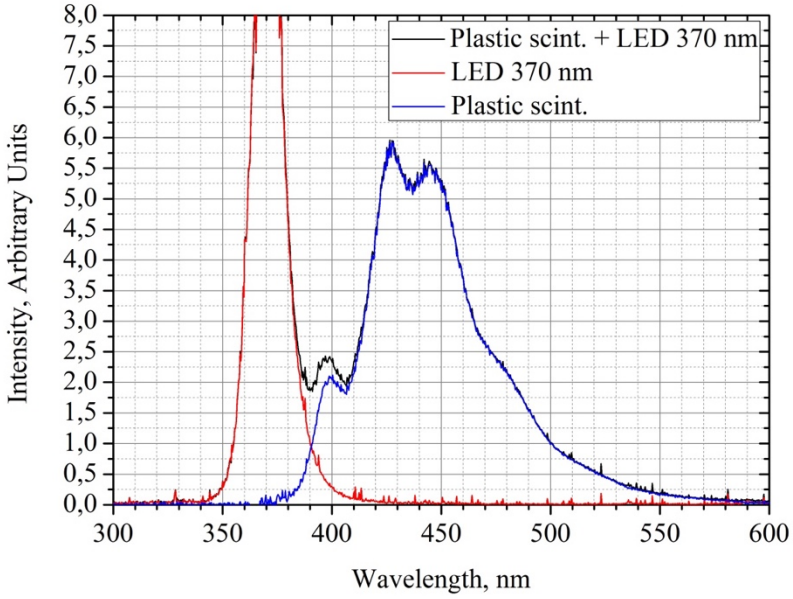

Fig. 3.7 Measured emission spectrum of the plastic scintillator.

4. The light output from scintillation materials

4.1 Energy calibration of the detectors

Energy spectra obtained with two scintillator materials, four radioactive sources and three biases fed to PMT (Fig. 4.1, 4.3) were analyzed. Because of the small size of the detector, the absorption of all gamma ray energy for most of the sources was unlikely. Thus, the full energy peak basically vanishes on the background. The Compton edges of the gamma ray spectra are however clearly visible. These were used in the detector energy calibration instead.

In Compton scattering a gamma ray scatters from a free electron. The energy of the electron is transferred to the detector while the scattered gamma ray escapes from the detector. The Compton electron has a well defined maximum energy, so called Compton edge, which corresponds to the maximum transferred energy from the gamma ray to the electron. This edge can be used for the energy calibration of the detector, and further, comparison of the light output from different detector materials.

To evaluate discrimination properties of detector materials, measurements with the same amount of material under the same conditions were provided.

Compton edge corresponds to the maximum energy transferred from scattered gamma to electron. Using kinematic equation of energy conservation law (1.2) and taking into account that maximum transferred energy will have backscattered gamma ($\theta = 180^{\circ}$) Compton edges of backscattered gammas could be calculated. Table 4.1 shows all calculated values of Compton edges for backscattered gammas used in the experiment.

In this work three radioactive sources were used for energy calibration. These sources were Na-22, Co-60, Cs-137. Based on gamma ray energies taken from [23] and that the rest mass of an electron is equal to 510,998 keV/c^2 one could calculate Compton edge energy T for all sources. Both Na-22 and Co-60 sources have two gamma rays to be considered in the calculations of Compton edge. The gamma ray with energy 511 keV emitted from Na-22 produces a Compton edge which is hard to locate on the spectra (Fig. 4.1, 4.3) from the background noise and therefore was not taken into account. The final result for Co-60 contains an average energy of two Compton edges.

Using an ideal detector with infinitely good resolution one could obtain spectra with vertical Compton edge. In this work spectra with inclined Compton edge were obtained. This smearing is due to the limited resolution of the detector system. The plastic scintillation material seems to have a slightly better energy resolution, which is seen from the sharper Compton edges in the

spectra shown in figures 4.1 and 4.3. It is however difficult to extract a numerical estimate for resolution. To find channel, which is proportional to Compton Edge energy on these figures middle point where the slope drops to half of the value of Compton peak.

Table 4.1 Calculated values of Compton edges of backscattered gammas.

Source	Branching, %	Gamma Energy, keV	Compton Energy, keV
Na-22	99,941	1274,5	1061,67
Co-60	99,85 99,9826	1173,228 1332,492	Aver. 1040,79
Cs-137	85,1	661,657	477,334

Minimal energy of photon, which could be recorded with data acquisition system was equal to the noise level in the signal and could not be zero. Average noise was approximately 3 ch. It also has to be noted that the energy spectrum has an offset. The channel corresponding to energy E = 0 keV is larger than 0, see Fig 4.2 and 4.4. More than one calibration point is needed to see this. For this calibration will be enough to have energy spectra of Na-22, Co-60 and Cs-137 Fig.4.1 – Fig.4.4.

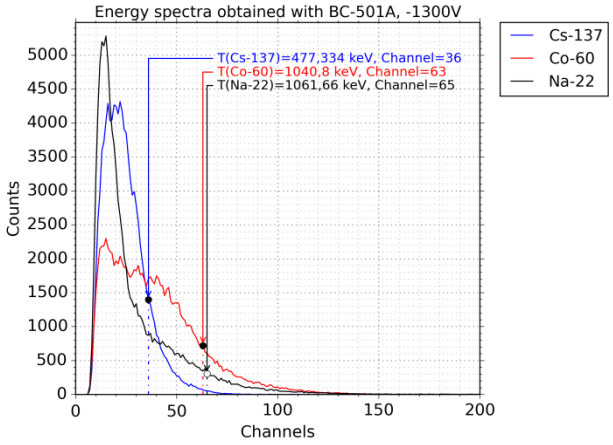

a)

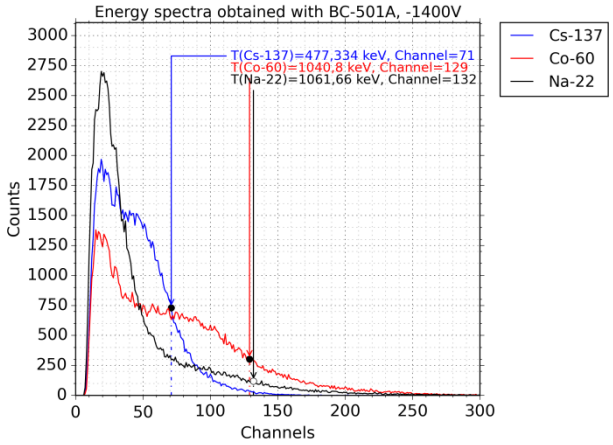

b)

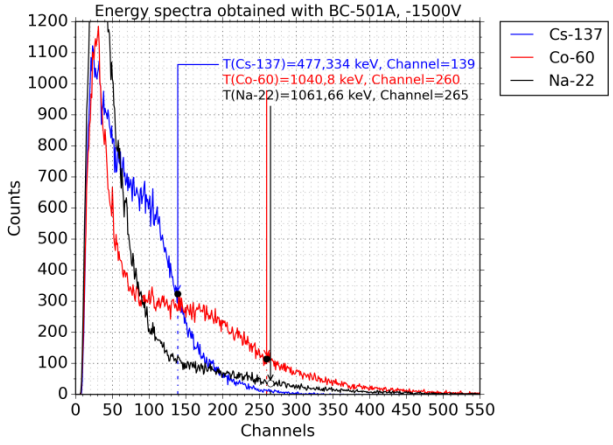

c)

Fig. 4.1 Energy spectra of Na-22, Co-60 and Cs-137 obtained with the liquid BC-501A scintillator. a) under -1300V bias, b) under -1400V bias and c) under -1500V.

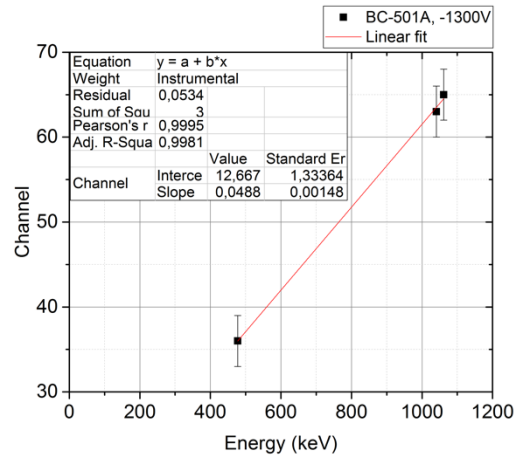

a)

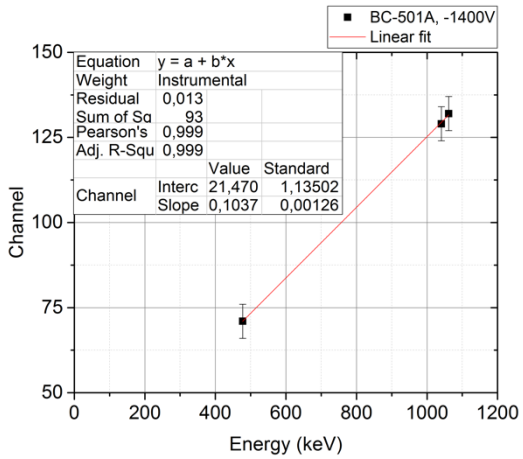

b)

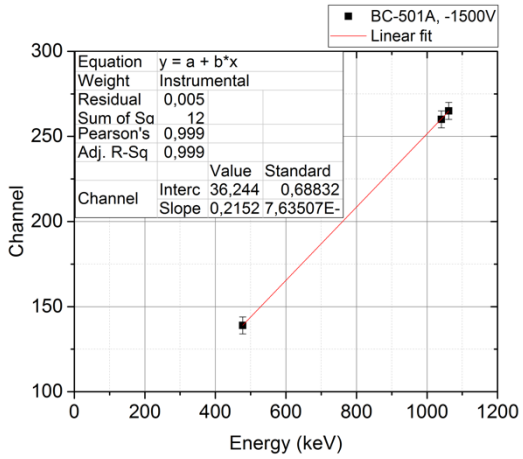

c)

Fig. 4.2 Energy calibration via linear fit to the data points which correspond to the Compton edges in the Fig. 4.1 a) under -1300V bias, b) under -1400V bias and c) under -1500V.

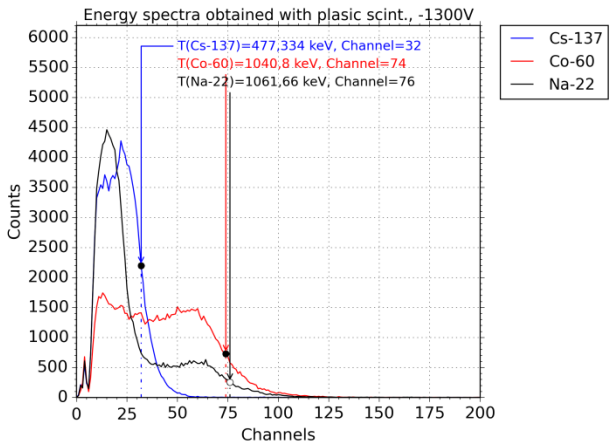

a)

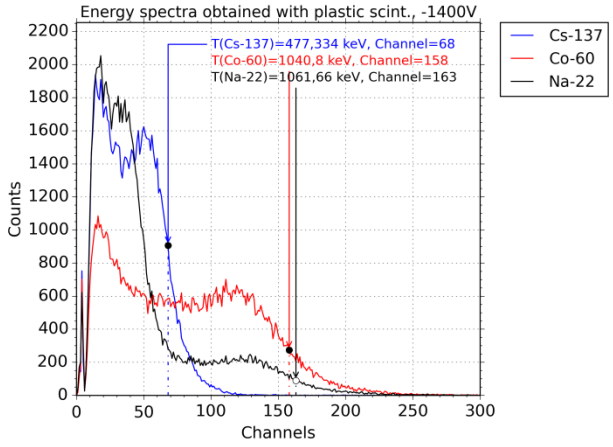

b)

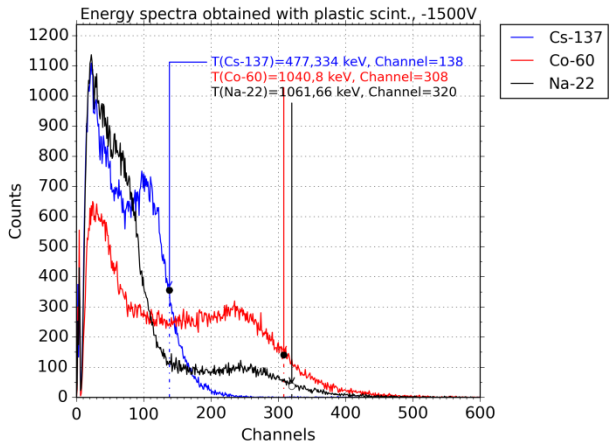

c)

Fig. 4.3 Energy spectra of Na-22, Co-60 and Cs-137 obtained with the plastic scintillator. a) under -1300V bias, b) under -1400V bias and c) under -1500V.

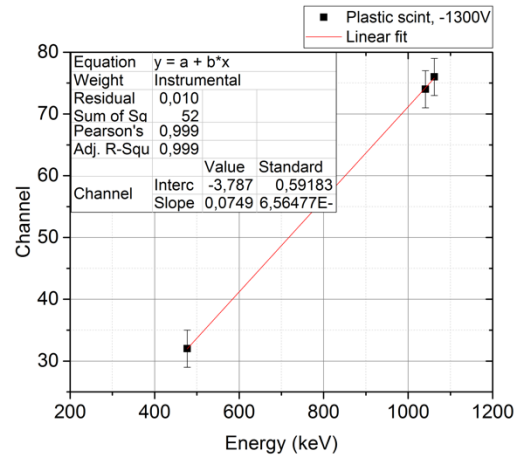

a)

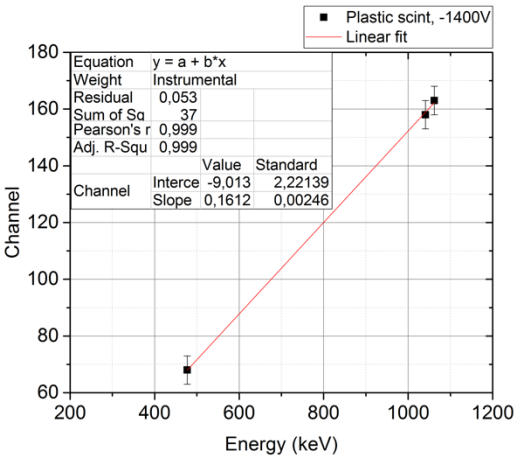

b)

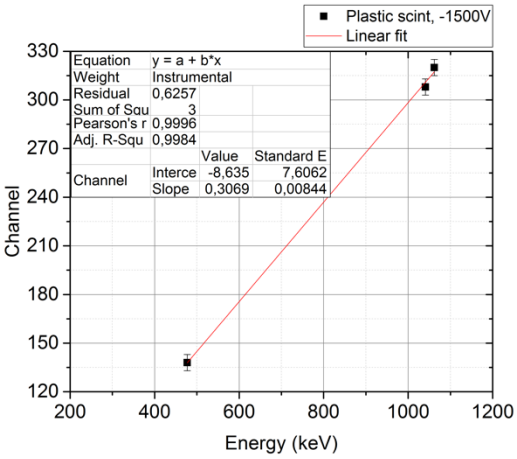

c)

Fig. 4.4 Energy calibration via linear fit to the data points which correspond to the Compton edges in the Fig. 4.3 a) under -1300V bias, b) under -1400V bias and c) under -1500V.

4.2 The PMT gain calibration

An important step of scintillation light yield measurement was the gain calibration of the photomultiplier tube. A LED based calibration system shown in Fig 4.6 - 4.8 was constructed for this purpose. A LED with wavelength 412 nm was selected for the gain calibration. The LED wavelength 412 nm is close to the maximum wavelength of scintillation emission spectra shown in figures 3.3. and 3.4. Precise wavelength measurement of the LED was carried with OceanOptics USB2000 spectrometer (Fig. 4.5). The LED's light power was measured with a micro power meter Thermopile Model 17S to find a number of emitted photons.

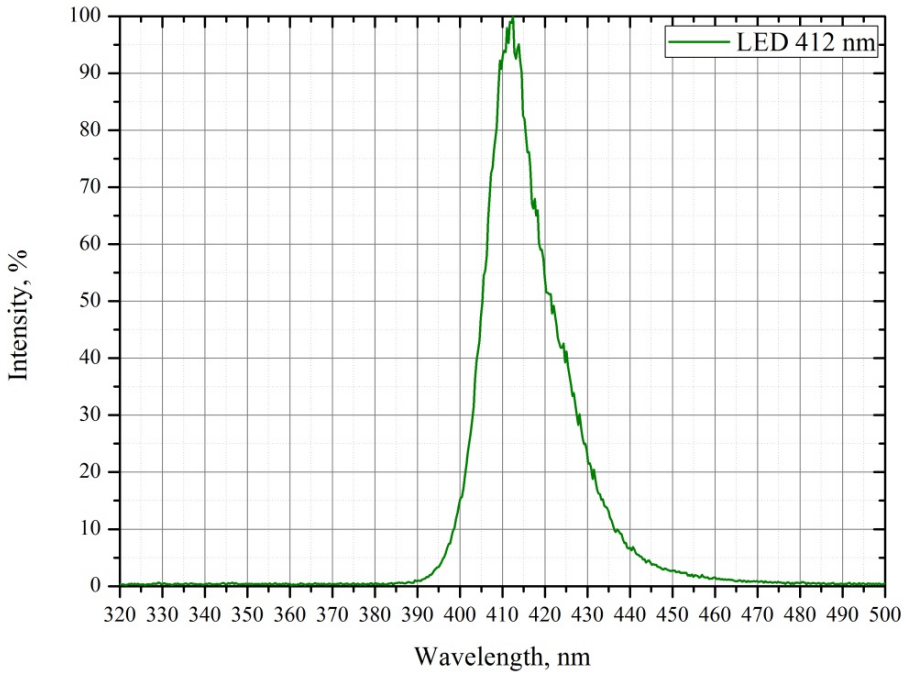

Fig. 4.5 Wavelength spectrum of the LED used in gain calibration (LED 412 nm).

As it shown in the Fig. 4.8 the LED calibration system consists of: LED, diaphragm, and a set of attenuation filters. These are mounted in a light tight case made of 1 cm thick polyvinyl chloride, which can be assembled on the top of the PMT. The diaphragm is used to ensure viewing angle of 15˚ and that all light would hit on the photomultiplier photocathode. Neutral density filters with different attenuation coefficients can be used to adjust the amount of light reaching the photocathode. The total attenuation coefficient of 10^6 was needed in these measurements. It was achieved with three neutral density filters. Each of these filters has 10^2 attenuation coefficient.

The PVC case was designed and machined at JYFL. The main criteria for the manufacture of the housing were to cover the full photocathode surface by the LED light, be able to change distance

between the LED and the photocathode, and have sufficient space for three neutral density filters.

Fig. 4.6 Cut view of the LED calibration system attached to the PMT (3D model).

Fig. 4.7 Photo of the LED calibration system.

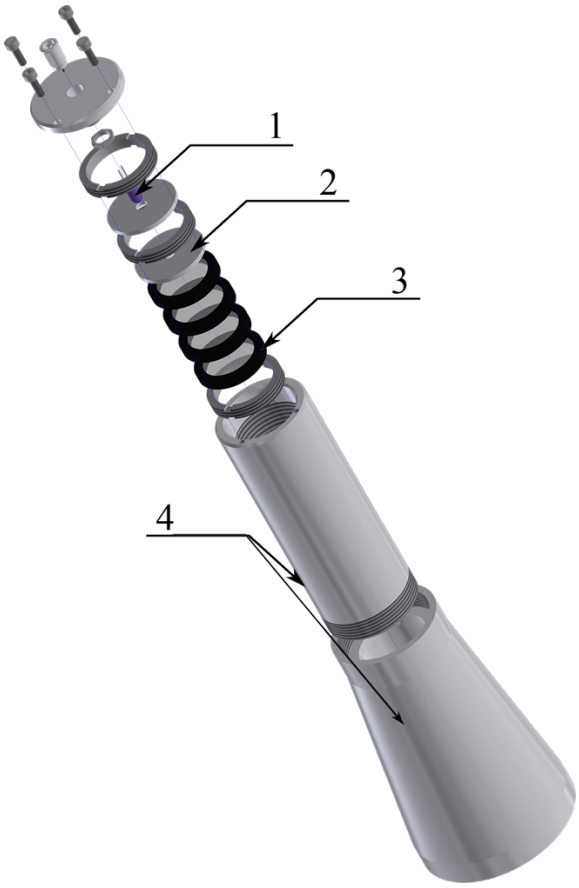

Fig. 4.8 Exploded view of the LED calibration system. 1 – LED 412nm, 2 – Diaphragm, 3 – Neutral density filters, 4 – Body.

The LED calibration system was placed on top of the PMT. To ensure constant output power of the LED, diode was always fed with the same 6 V power supply. The anode current of PMT was measured with Keithley 6485 picoammeter. For one PMT bias value 100 anode current values were recorded. The average current values for each step of bias are shown in Table 4.2.

The gain of the PMT was determined by comparison of an anode current with a photoelectron current of the PMT under the different values of bias. To measure anode current the picoammeter was used. The photoelectron current was recalculated based on the number of photons fallen on the photocathode.

Table 4.2 Anode current of Hamamatsu R1828-01 connected to Ortec 269.

Bias, V	Anode current, μA	Standard deviation, μA
-1200	-10,08	0,03
-1300	-22,72	0,05
-1400	-47,28	0,04
-1500	-92,99	0,05
-1600	-177,24	8,68

It was assumed that the number of photons fallen on the photocathode was equal to the number of photons emitted by the LED. The number of photons emitted by the LED was found using a light power of the LED. The light power was measured with the micro power meter. The measured value value was 4,5 ± 0,1 mW within viewing angle of 15˚. Each photon from the diode has average energy E:

$$E = \frac{h \cdot c}{\lambda}; \tag{4.1}$$

where h is Planck's constant $6{,}62606957 \cdot 10^{-34}$ J·s, c is speed of light 299792458 m/s and λ is the average wavelength of the photons emitted from the LED. Using this average energy, it is possible to find a number of photons N per second emitted from the LED:

$$N = \frac{P \cdot 10^{-6}}{E}; \tag{4.2}$$

where P is the LED light power and E is the average photon energy. Substituting values into equations (4.1) and (4.2) one could obtain $N = (9{,}33 \pm 0{,}21) \cdot 10^{9}$ photons/s, including the attenuation (10^{6}) of the gray filters.

Using quantum efficiency of the photocathode given by the manufacturer Fig. 4.9 [16], the photocurrent generated by the photons emitted from the LED was determined.

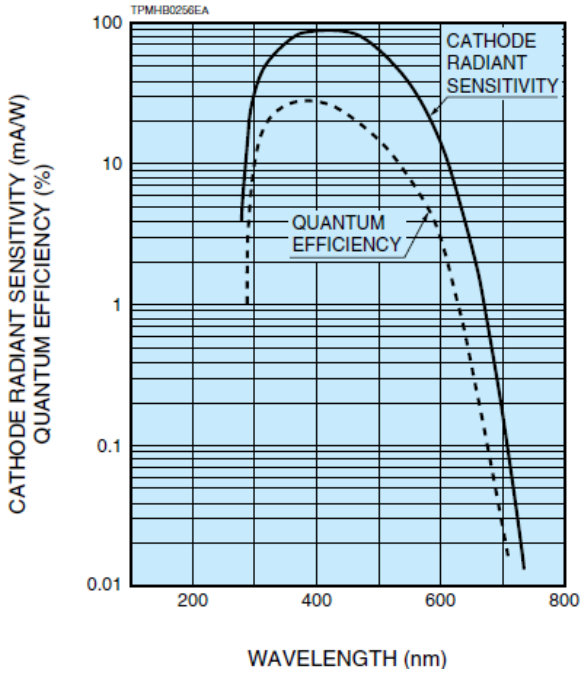

Fig. 4.9 Typical spectral response of Hamamatsu R1828-01 PMT [16].

Fig. 4.9 shows that 412 nm wavelength corresponds to 29 % of quantum efficiency. Full width half maximum of the wavelength distribution of the LED is 16 nm (Fig. 4.5). The half maximum values are 405 and 421 nm. In this range, the quantum efficiency varies between 28 and 29 %. 29 % is used for calibration. This quantum efficiency value was used to convert the number of photons obtained above to the photocathode current $I_K = (-433{,}7 \pm 9{,}6) \cdot 10^{-12}$ A.

The gain of the PMT could be directly found from the anode and photocathode currents of the photomultiplier tube. (Table 4.3 and Fig. 4.10).

Table 4.3 Measured gain of the Hamamatsu R1828-01 PMT.

Bias, V	Gain, $\cdot 10^3$	Error, $\cdot 10^3$
-1200	24,1	0,5
-1300	54,3	1,2
-1400	112,9	2,5
-1500	222,1	4,9
-1600	423,3	22,8

The deduced gain values were compared with the data given by the manufacturer [16]. The gain curve given by Hamamatsu is shown in Fig. 4.11. The comparison showed slight difference. The measured gains were about factor of 2 smaller than manufacturer's values.

The measured gain values were used for light yield calculation.

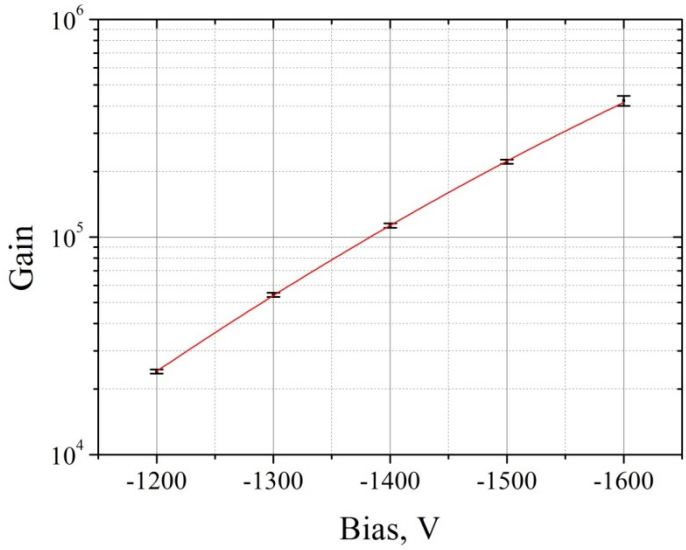

Fig. 4.10 Measured gain of the Hamamatsu R1828-01 PMT.

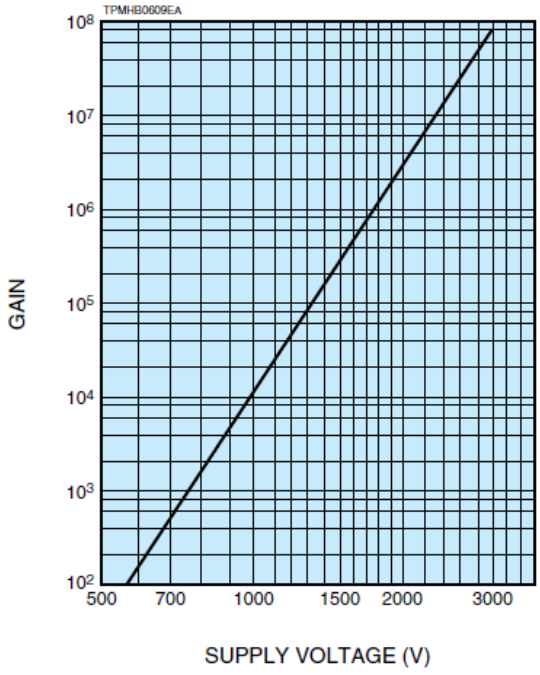

Fig. 4.11 Typical gain characteristics of PMT Hamamatsu R1828-01 [16].

4.3 Light output of the studied materials

The process of light yield determination is complicated, because the light yield depends on many parameters of the investigated system. These parameters include the dimensions of a scintillation material, optical properties of a scintillator, sensitivity of a PMT to a scintillation light, efficiency of a PMT and others [24].

For determination of scintillation light yield the Pulse method was used [25], which arises from basic principles of scintillation counters described in [10] and [26]. A schematic view of a scintillation counter used in this work shown in Fig. 4.12

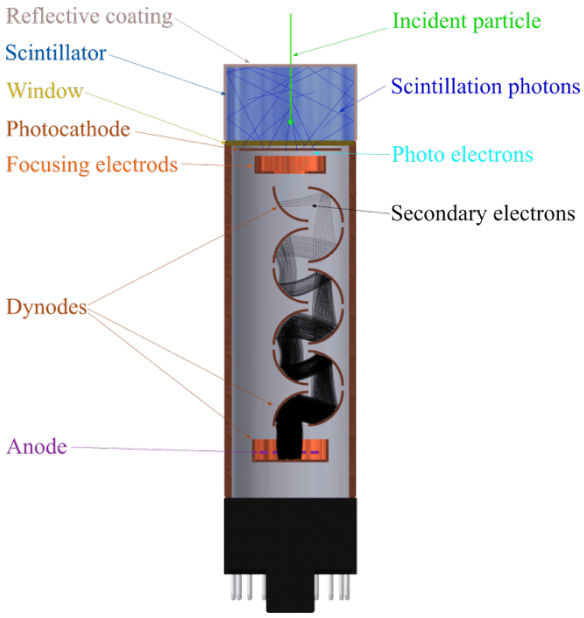

Fig. 4.12 Schematic view of a scintillation counter.

Scintillation light is generated by the interaction of the incoming radiation with the scintillation material. This light is emitted in all directions. To collect all this scintillation light on the photocathode of the PMT and prevent escaping of the light, both scintillation materials were covered with aluminum (the plastic scintillator was covered with a reflective paint and an aluminum foil; the liquid scintillator was stored in the aluminum vessel).

For light yield counting the light collection model described in [13, 14] was used. This model was simplified, to satisfy the goals of this work. It was assumed that scintillation light was not absorbed in scintillator and there were no loses due to light reflection, in other words all the photons emitted from the scintillator reached photocathode of the PMT. This is known not be true, but the losses are not known well enough to consider in detail. Assuming similar losses of light in the scintillation material samples, a meaningful comparison between the materials can be made.

The photon-irradiated photocathode emits photoelectrons. The amount of photons reached photocathode and a number of emitted electrons have the following dependence:

$$N_K = \eta \cdot N_{ph}; \tag{4.3}$$

where N_{ph} is number of incident photons, N_K is a number of emitted photoelectrons and η is the quantum efficiency.

The emitted photoelectrons are accelerated and focused to the first dynode. The impact of the accelerated photoelectrons causes emission of secondary electrons. The secondary electrons are accelerated again and hit next dynode releasing secondary electrons. This process continues until re-emission from the last dynode. The electrons from the last dynode are collected on the anode. The amount of secondary electrons from the dynode surface is larger than amount of the incident electrons. The ratio between the amount of emitted and incident electrons in single dynode is called secondary emission ratio, which depends on kinetic energy of incoming electrons and properties of the dynode material. Secondary emission allows obtain a cascade multiplication of photoelectrons in a PMT. Multiplication factor μ between the amount of electrons released from the photocathode and amount of electrons which reached the anode is called the gain.

$$N_P = \mu \cdot N_K; \tag{4.4}$$

where N_P is a number of electrons reached anode and μ is the gain.

The current signal from the anode is recorded as a voltage signal.

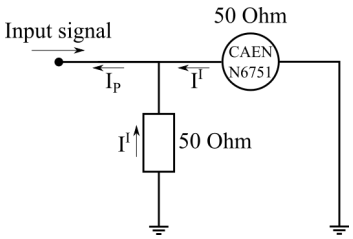

Fig. 4.13 Electric circuit of the experimental setup

To find a number of anode's electrons reflected in a pulse thee fallowing equation was used:

$$N_P = \frac{2 \cdot \int_{t_1}^{t_2} V dt}{Z \cdot e}; \tag{4.5}$$

since the all signals were digitized the integral in the equation 4.5 was replaced with the sum:

$$N_P = \frac{2 \cdot \sum_{i=M}^{N} (V_i \cdot t)}{Z \cdot e}; \tag{4.6}$$

where M is an index of the first channel in the pulse, N is an index of the last channel in the pulse, V_i is a voltage value of a single channel, t is a time sample width and Z is impedance of digitizer.

Substituting equation 4.6 into equations 4.4 and 4.3, a number of scintillation photons emitted on the photocathode could be found:

$$N_{ph} = \frac{2 \cdot \sum_{i=M}^{N} (V_i \cdot t)}{Z \cdot e \cdot \mu \cdot \eta}; \quad (4.7)$$

For each case, the technique was applied to pulses at the Compton edge in the corresponding gamma ray spectrum. This way the amount of energy left in the scintillator was known in a reasonable accuracy.

To verify the consistency of the method described above and increase overall statistics, light yield of both scintillators was determined under all the three sources used (Na-22, Co-60 and Cs-137) under the three bias values applied to the PMT. It is recalled here that both scintillators had the same dimensions ∅50,5mm×25mm. Obtained light yield values for the liquid and the plastic scintillators are present in tables 4.4 and 4.5 correspondingly.

Table 4.4 Deduced light yield of the BC-501A liquid scintillator.

Source	Na-22			Co-60			Cs-137		
Negative Bias	1300V	1400V	1500V	1300V	1400V	1500V	1300V	1400V	1500V
Light yield, ph/keV	9,6 ± 1,07	9,16 ± 0,57	8,99 ± 0,48	9,15 ± 0,87	8,86 ± 0,71	8,82 ± 0,56	9,76 ± 1,52	10,37 ± 1,28	10,38 ± 1,05

Table 4.5 Deduced light yield of the plastic scintillator.

Source	Na-22			Co-60			Cs-137		
Negative Bias	1300V	1400V	1500V	1300V	1400V	1500V	1300V	1400V	1500V
Light yield, ph/keV	16,25 ± 1,41	15,81 ± 1,08	16,24 ± 0,26	15,91 ± 1,51	15,73 ± 1,36	16,71 ± 1,61	13,63 ± 2,11	16,19 ± 2,11	15,27 ± 1,82

From the tables above one could conclude that the average light yield of the liquid BC-501A scintillator is 9,45 ± 1,19 ph/keV. Plastic scintillator has 15,75 ± 2,23 ph/keV, which is 167% of light yield of BC-501A.

Obtained light yield for BC-501A is higher than 2,03 ± 0,06 ph/keV published by Moszynski in [27] for scintillator with dimensions ∅50mm×50mm. This difference can may be explained by difference of the equipment. Comparison with SaintGobain datasheets showed just opposite that the current measurement of the light yield value is slightly lower than manufacturer's value. It is stated in [28] and [29] that BC-501A scintillator light output is 78% of that of anthracene, anthracene light output is 40-50% of light output of NaI(Tl) and NaI(Tl) light yield is 38 ph/keV, which eventually gives that BC-501A has a light yield 11,86 – 14,82 ph/keV.

5. Detection efficiency

To calculate geometrical efficiency of the constructed scintillation detectors, the dimensions of the detectors and the distance from the source (130 mm) were substituted to solid angle equation [9, p.118]:

$$\Omega = 2\pi\left(1 - \frac{d}{\sqrt{d^2+a^2}}\right) \tag{5.1}$$

where Ω is solid angle, d is distance between source and detector and a radius of detector. In the measurements in this work Ω equals to 0,11 rad. Geometrical efficiency is defined as:

$$\varepsilon_{geom} = \frac{\Omega}{4\pi} \tag{5.2}$$

The geometrical efficiency of the experimental setup was ε_{geom} = 0,89%. Since all measurements were made in the same geometry this efficiency can be used for all measurements.

Geometrical efficiency tells the probability that the radiation hits the detector. Other efficiencies that include also the interaction with the detector are Total and Intrinsic Efficiency. Values of these can be found using calibrated sources. In the current experiments, the total and intrinsic efficiencies were determined with a calibrated Cs-137 source. At 03.03.89 activity of Cs-137 source was 34,83 kBq. Where the measurement with plastic scintillator took place at 03.06.14, recalculated activity was 19,47 kBq. The measurements with liquid BC-501A scintillator were made at 15.07.14, here recalculated activity was 19,42 kBq. 108309 events were recorded in 28 min 08 s. Background rate in this measurement was 10,7 counts/s. After subtracting background 90247 events were obtained in 1688 s with plastic scintillator. 100056 events were recorded in 23 min 54 s with liquid scintillator with the background radiation rate 10,8 c/s that give 84569 events in 1434 s. These data could be substituted into the following equations from [9] to calculate Total and Intrinsic efficiency:

$$\varepsilon_{tot} = \frac{number\ of\ registered\ events}{number\ of\ emited\ gammas} \tag{5.3}$$

$$\varepsilon_{int} = \frac{number\ of\ registered\ events}{number\ of\ gammas\ emited\ \ on\ the\ detector} \tag{5.4}$$

For the detector with the plastic scintillator and for detector with the liquid BC-501A scintillator the next values of total and intrinsic efficiencies ε_{tot} = 0,27%, ε_{int} = 30,85% and ε_{tot} = 0,30%, ε_{int} = 34,12% were obtained correspondently.

6. Gamma-neutron discrimination properties

All data were analyzed in off-line mode using Charge Comparison Method (CCM) [8, 30]. The same method was applied by Flaska in [31], by Lintereur et al. in [32] and in [33]. This method allows find differences between pulses generated by gammas and neutrons applying integration of certain time intervals of the pulses. For data analysis a program code was written in Python (full code is presented in Appendix 2). As a particular example a part of the code which realizes CCM is presented in Table 6.1.

Table 6.1. Realization of CCM in Python.

```
data = [[pulse_1], [pulse_2], ...]

a = -20
b = 150
c = 13

for item in data:
        pos_of_max = item.index(max(item))
        pulse_start = pos_of_max + a
        pulse_end = pos_of_max + b
        pulse_integral = sum(item[pulse_start:pulse_end+1])
        pulse_integral_list.append(pulse_integral)
        tail_start = pos_of_max + c
        tail_integral = sum(item[tail_start:pulse_end+1])
        tail_integral_list.append(tail_integral)
        tail_to_total_ list.append(tail_integral/pulse_integral)
```

The typical pulse shape and integrating regions are shown in Fig. 6.3. Initially the signal amplitude had a negative value; during processing the signal was inverted. The initial negative signal results from the negative current (Fig. 4.13) in the circuit. The direction of current is considered to be opposite to the direction of free moving electrons in a conducting wire. Since anode collects secondary electrons and becomes negatively charged, the current in the circuit directed from the digitizer towards the anode.

The pulses generated by both gammas and neutrons look quite similar, and contain fast rise time and slow decay time (Fig. 6.1, Fig. 6.2). The excitation produced in the scintillator by gamma rays decays slightly faster than those produced by neutrons. Therefore, the relative intensity of the tail part of the pulse can be used to identify the particle that caused the excitation. The ratio of the area of the tail of the signal (tail integral) and the total area of the signal (total integral) is thus different for neutron pulses and gamma pulses. These values were used in PSD analysis.

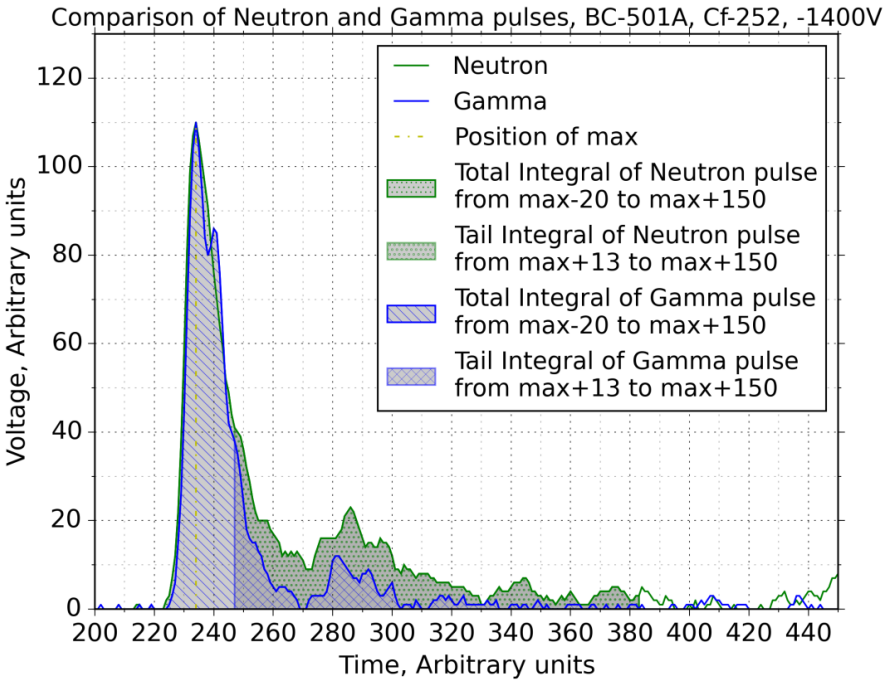

Fig. 6.1 Comparison of neutron and gamma pulses extracted from Neutron and Gamma areas of PSD spectra obtained with the liquid BC-501A scintillator.

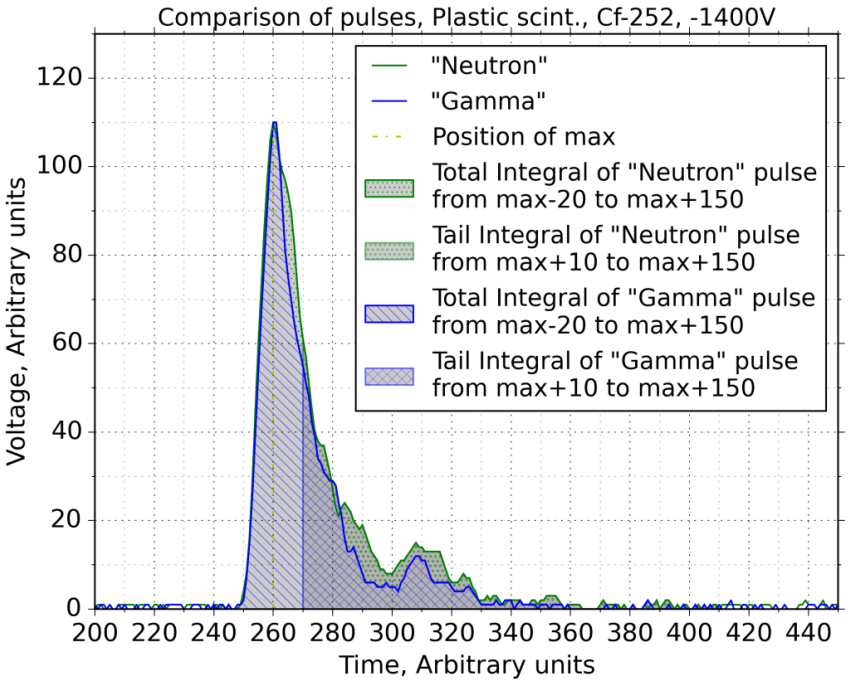

Fig 6.2 Pulses obtained after application the same comparison technique to PSD spectra of plastic scintillator.

Maximum of the pulse (Fig. 6.3. max) was taken as reference point for delimitation of time borders. Time intervals were defined for each source/scintillator individually, to provide better discrimination efficiency. Commonly start point of Total area was placed 10 – 15 ns (Fig. 6.3 max+a) earlier than the maximum of the pulse, start point of Tail area 10 – 30 (Fig. 6.3 max+c) ns later than the maximum and end point was common for both area and placed 75 – 150 ns (Fig. 6.3 max+b) after the maximum.

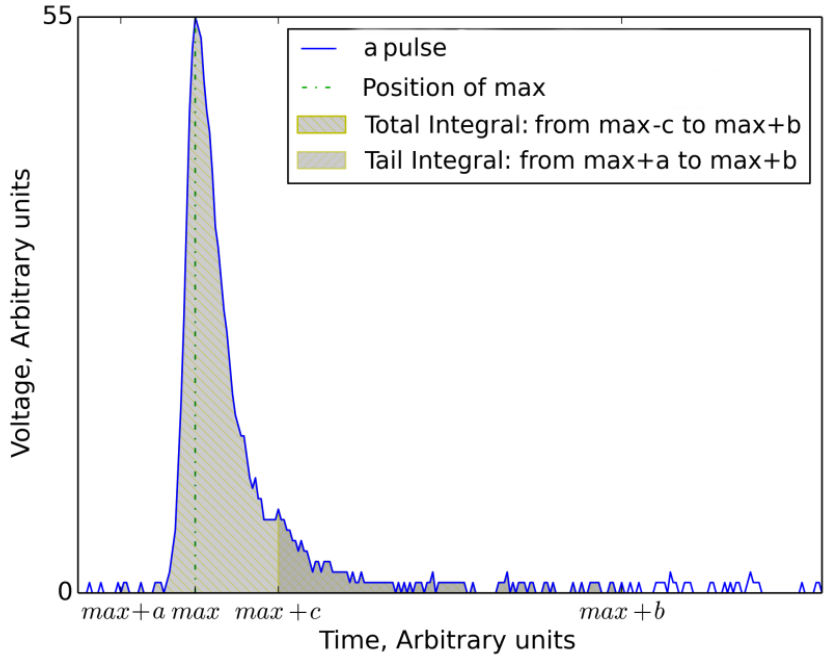

Fig. 6.3 Typical inverted single pulse recorded from liquid BC-501A scintillator and Na-22 source, applying bias =-1300 V to PMT base. This figure shows Total and Tail areas of pulse integration.

To guarantee the same statistic the equal amount of pulses (100000) from each measurement were analyzed. In these measurements a Cf-252 source was used. A Cf-252 source is a good emitter of neutrons, emitting 3,75 neutrons/fission [34]. The source also emits gamma rays. These gamma rays are following the alpha decay of californium, and in particular, the decay of neutron rich fission products from the fission branch of californium decay. Fig 6.4 shows decay scheme of Cf-252. In these measurements the same range of bias voltages as for energy calibration (Chapter 4.1) was used. The PSD method described above was applied to distinguish between neutrons and gamma rays.

Figures 6.6 – 6.9 show two methods to distinguish between neutrons and gammas. In the Fig 6.6 and 6.8 one dimensional spectrum “Tail-to-total ratio vs. Pulse height” is shown. In the Fig. 6.6 the peak ~0,2 corresponds to the gamma rays, whose signal has a weaker long-lived component,

while the peak at ~0.4 corresponds to neutrons. The peaks can be identified by making the same discrimination to the data collected with Cs-137 source that emits only gamma rays.

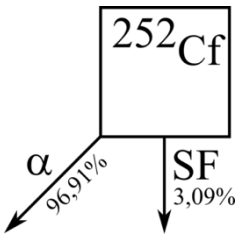

Fig. 6.4 Decay scheme of Cf-252.

In Fig. 6.8 a) – c) it is impossible to find peaks that might correspond only either to gamma rays or to neutrons. Also in these figures a small peak around 0,8 ratio is observed. This peak was caused by a signal containing noise. A sample of such signals is shown in Fig. 6.5.

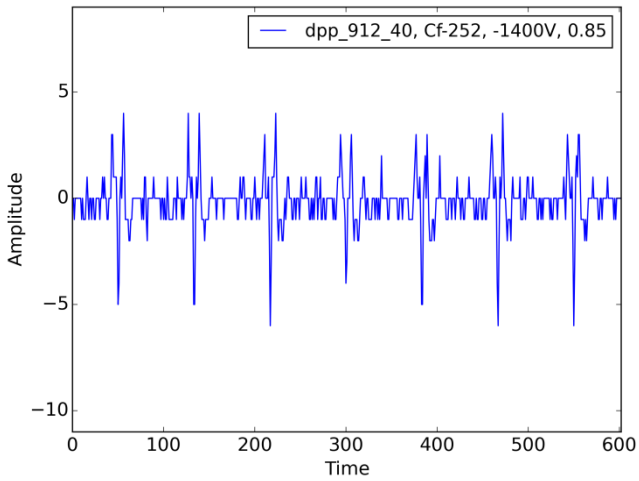

Fig. 6.5 Sample of a signal with high noise ratio. This signal was obtained from the plastic scintillator and Cf-252 source under -1400V bias. Tail integral: max+20/max+170, total integral: max-20/max+170. Tail to total ratio for this signal is 0.85.

The one-dimensional discrimination is not fully satisfying since the peak in the spectrum of ratios overlap and do not allow an unambiguous assignment of events. In the Fig. 6.6 and Fig 6.8, the same pulse quantities are plotted in a two-dimensional histogram, “Total integral vs. Tail integral”. Figures 6.6 a) – c) show two clearly separated groups, the upper groups correspond to neutrons and the lower groups to gamma rays. Although these groups are not completely separated either, the two-dimensional histogram allows much better discrimination between gamma rays and neutrons: the number of not resolved events is much smaller. The two-dimensional spectra in figures 6.8 a), b), c) also reveal that the studied plastic scintillator has essentially no gamma/neutron discrimination properties.

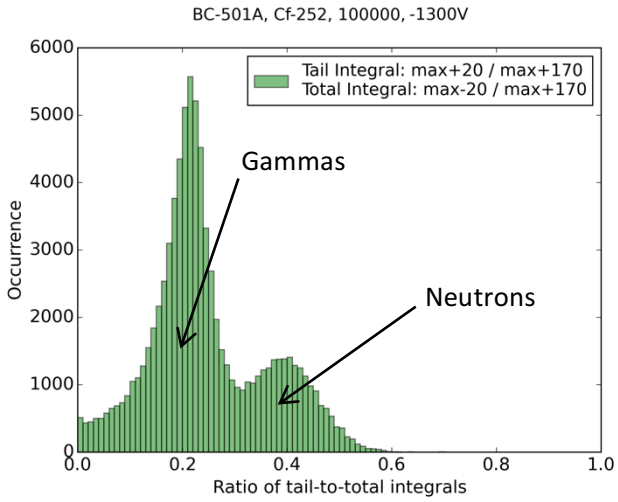

a)

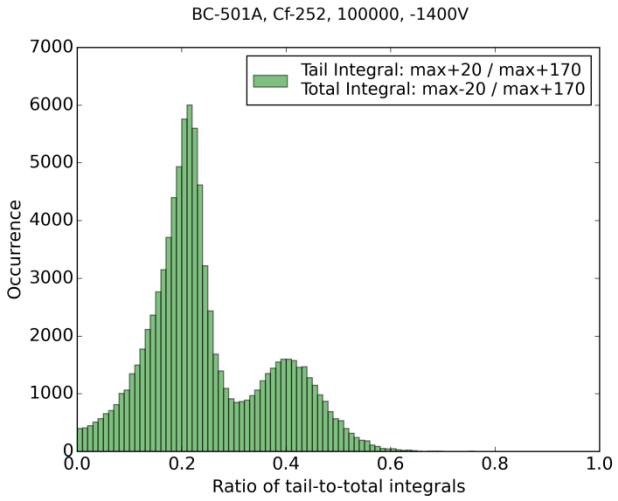

b)

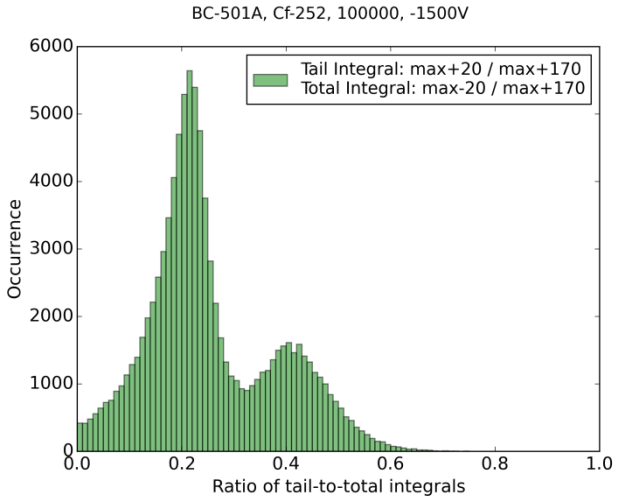

c)

Fig. 6.6 Histograms of tail-to-total ratio for the liquid BC-501 scintillator. Cf-252 radioactive source, 100000 counts. a) under -1300V bias, b) under -1400V bias and c) under -1500V.

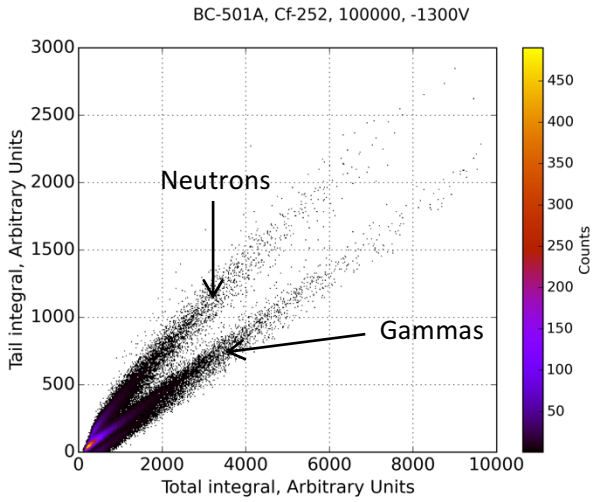

a)

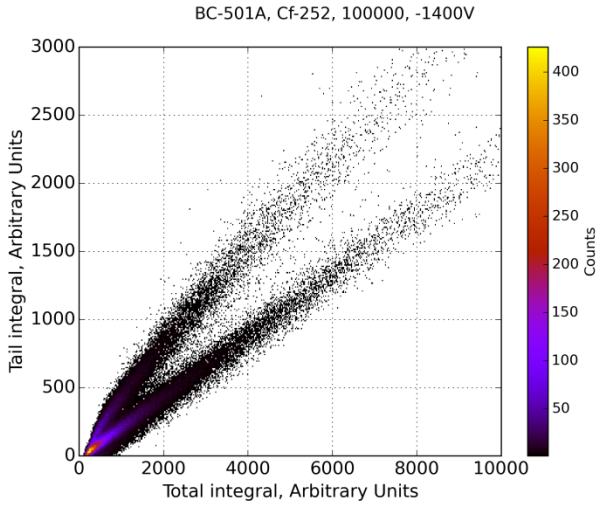

b)

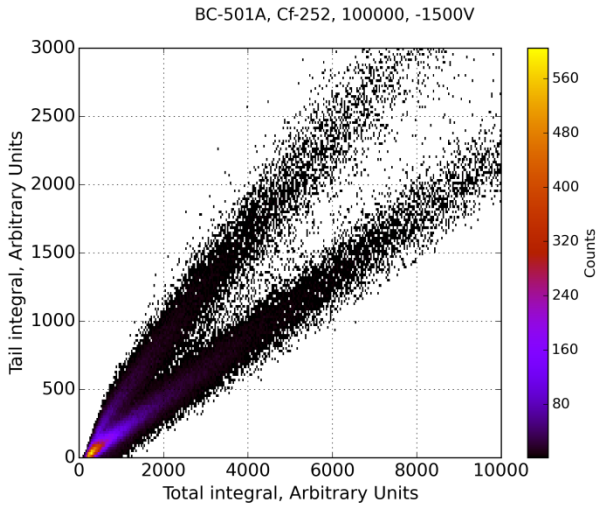

c)

Fig. 6.7 2D histograms of Total integral vs. Tail integral for the liquid BC-501 scintillator. Cf-252 radioactive source, 100000 counts. a) under -1300V bias, b) under -1400V bias and c) under -1500V.

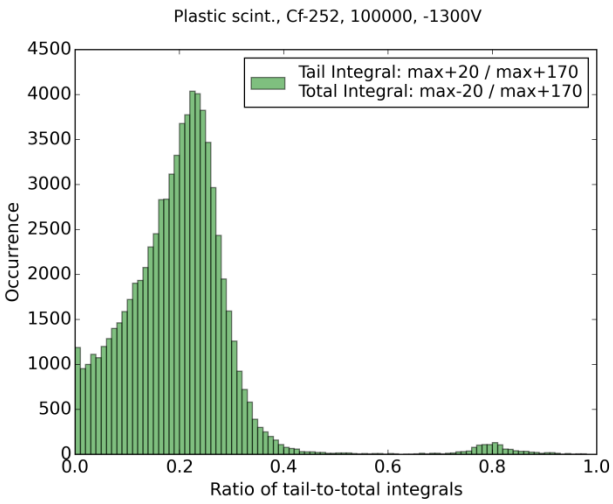

a)

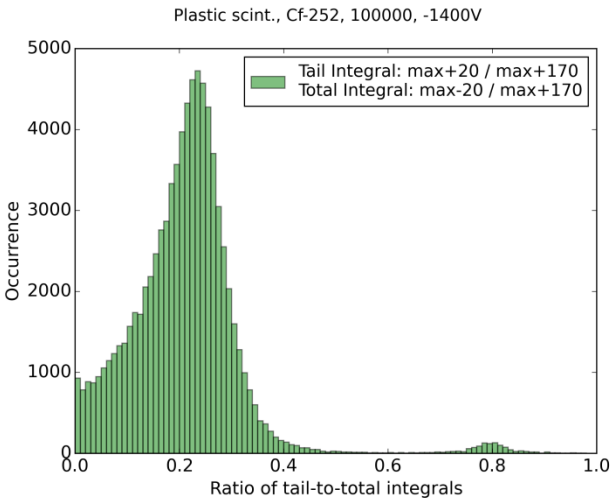

b)

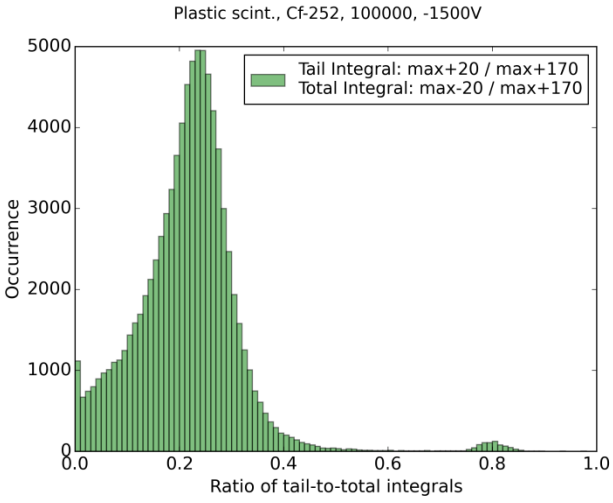

c)

Fig. 6.8 Histograms of tail-to-total ratio for the plastic scintillator. Cf-252 radioactive source, 100000 counts. a) under -1300V bias, b) under -1400V bias and c) under -1500V.

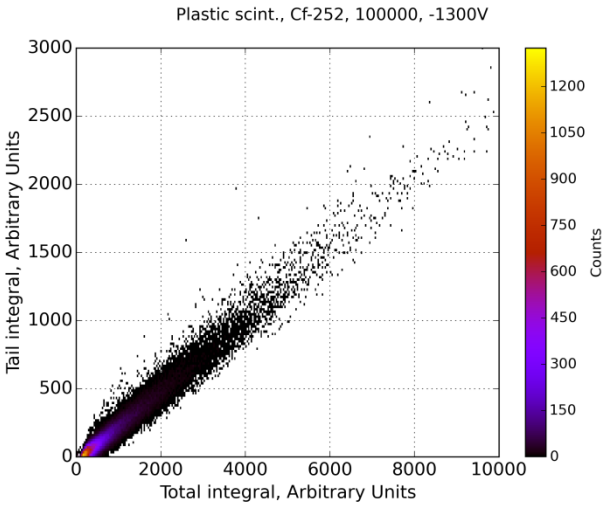

a)

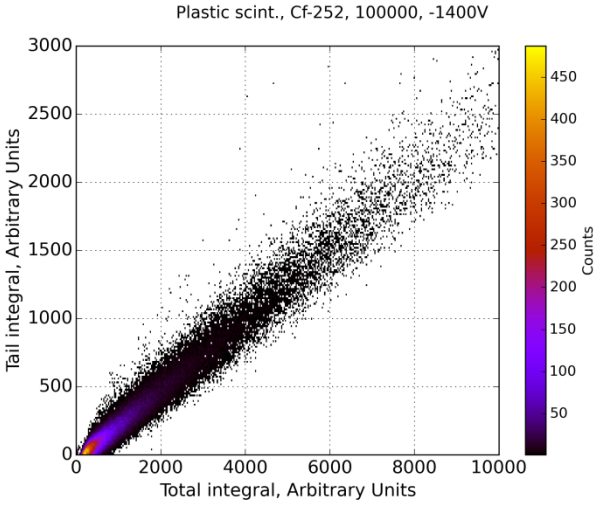

b)

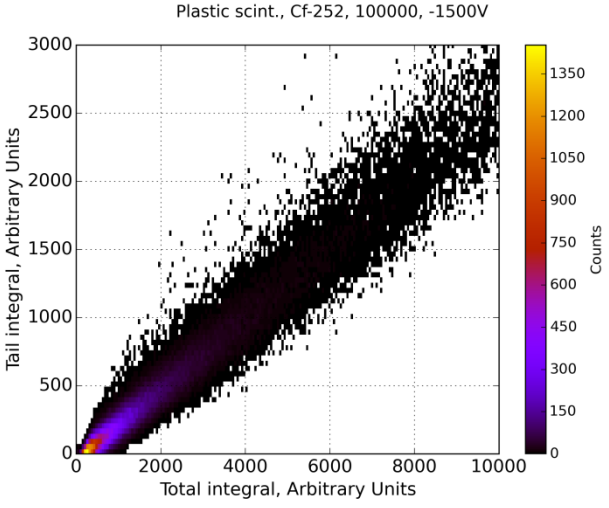

c)

Fig. 6.9 2D histograms of Total integral vs. Tail integral for the plastic scintillator. Cf-252 radioactive source, 100000 counts. a) under -1300V bias, b) under -1400V bias and c) under -1500V.

The dependence between pulse shape discrimination properties reflected in histograms (Fig. 6.6 a) – c)) obtained with the liquid BC-501A scintillator and the all PMT bias values was evaluated with figures of merit (FOM):

$$FOM = \frac{\Delta S}{FWHM_1 + FWHM_2}; \quad (6.1)$$

where ΔS is difference between peaks maxima, FWHM1 and FWHM2 are full width at half maxima of the gamma and the neutron peaks correspondingly (Fig. 6.10). FOM is a measure of how well neutrons and gammas can be separated.

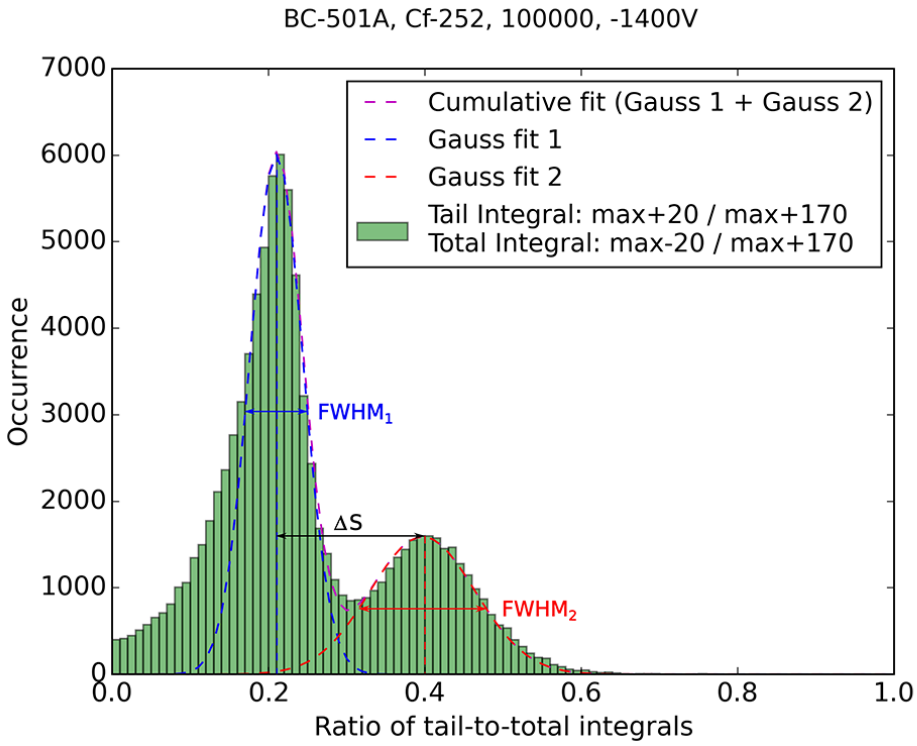

Fig. 6.10 Figure of merit for gamma – neutron pulse shape discrimination.

Obtained FOM values are presented in table 6.2. These values do not have significant differences for the all voltages applied to the PMT.

Table 6.2. FOM for PSD histograms obtained with the liquid BC-501A scintillator.

Bias, V	FOM
-1300	0,86
-1400	0,77
-1500	0,83

Conclusion

Properties of a new plastic scintillation material were studied. Comparison was made to well known BC-501A liquid scintillator.

The scintillation light wavelength spectrum was measured with a spectrometer. To ensure sufficient light output for these measurements, the states of scintillation material were excited with a UV LED, instead of ionizing radiation.

Two scintillation detectors with similar dimensions and same photomultiplier tube were build from the two different scintillation materials. The intrinsic total efficiency of the built detectors was quite similar: 31 % for the plastic detector and 34 % for the BC-501A detector. On the other hand, the plastic detector seems to have slightly better energy resolution.

The light output of the detector was studied with gamma ray sources. The charge of amplified pulses corresponding the energy of the scattered Compton electron at the Compton edge was determined. The poor peak efficiency of the detectors together with low resolution made it impossible to use the full energy gamma peak. The gain of the PMT was calibrated with a LED light source, which allowed to determine the amount of photons released in the absorption of the energy of the Compton electron. The average light yield for BC-501A was determined as 9,5 ± 1,2 photons/keV. This is slightly lower than the ~13 photons/keV deduced from the manufacturer documentation. The light yield of the plastic material was determined as 15,8 ± 2,3 photons/keV. Assuming that the studied detectors are comparable, the light yield of the plastic is about 125 % that of anthracene.

The pulse shape discrimination spectra obtained with the BC-501A scintillator show that the experimental setup can distinguish between gammas and neutrons, if the material has discrimination properties. Liquid scintillation detector was found to have better discrimination properties as compared with the studied plastic detector. The plastic scintillation sample was not capable to discriminate between neutrons and gamma rays.

The pulse shape discrimination properties of the materials were studied using charge comparison method. The analysis was made off-line on recorded scintillation pulses. A Python program code was written for this analysis.

References

1. Stephen A. Dye, Survey of Instrumentation and Measurement, Wiley New York, USA, 2001
2. H. Kallmann, Natur und Technik, (July 1947)
3. I. Broser, Z. Naturforsch. 2s (1947) 439
4. H. Kallmann, Z. Naturforsch. 2s (1947) 642
5. J. Cooper, NOvA Conceptual design report, (2006)
6. M. Wurm Astroparticle Physics 35 (2012) 685 – 732
7. G. Bizard, Nuclear Physics News, 1, n 5 (1991) 15
8. F.D. Brooks, Development of organic scintillators, Nucl. Instrum. Meth. 162 (1979) 477
9. Glenn F. Knoll, Radiation Detection and Measurement, 4th ed., Wiley, New York, USA, 2010
10. J.B. Birks, The theory and practice of scintillation counting, Pergamon press, Oxford, Great Britain, 1967
11. S-O Flyckt et al., Photomultiplier tubes principles and applications, Photonis, Brive, France, 2002
    http://www2.pv.infn.it/~debari/doc/Flyckt_Marmonier.pdf
12. ANSI/IEEE Standard 398
13. T. Hakamota, et al (ed.), Photomultiplier tube basics and applications, 3rd ed,. Hamamatsu Photonics KK, 2007.
    www.hamamatsu.com/resources/pdf/etd/PMT_handbook_v3aE.pdf
14. Photomultiplier handbook Burle Idustries, 1980
    http://psec.uchicago.edu/links/Photomultiplier_Handbook.pdf
15. Rhys M. Preston, IEEE Transactions on nuclear science, Vol. 61, No. 4, August 2014
16. Technical documentation, PMT R1828-01, Hamamatsu Photonics K. K., 2010
    https://www.hamamatsu.com/resources/pdf/etd/R1828-01_R2059_TPMH1259E.pdf
17. Ortec PMT base 269
    http://www.ortec-online.com/download/269.pdf
18. The Andrzej Soltan Institute For Nuclear Studies, Euroball neutron detectors electronics ”Bartek” NDE 202, Serek 2001
19. Caen, Technical Information manual for digitizer N6751
    NPO: 00100/09:6751x.MUTx/08
    http://www.caen.it/servlet/checkCaenManualFile?Id=10611
20. P. Lombardi, Nucl. Instr. and Meth in Phys. Res. A 701 (2013) 133 – 144

21. Technical documentation, BC-501A liquid scintillators, Saint-Gobain (2005 – 14) http://www.crystals.saint-gobain.com/uploadedFiles/SG-Crystals/Documents/SGC%20BC501_501A_519%20Data%20Sheet.pdf
22. J.S. Lilley, Nuclear physics principles and application, Wiley, West Sussex, England, 2001
23. Richard B. Firestone Table of Isotopes, 8th ed., Wiley
24. M. Moszynski, IEEE Transactions on Nucleear Science, Vol. 44, No. 3, (June 1997)
25. E. Sysoeva, Nucl. Instr. and Meth in Phys. Res. A 486 (2002) 67-73
26. S.E. Derenzo, Scintillation Counters, Photodetectors and Radiation Spectroscopy, IEEE Short Course Radiation Detection and Measurement, 1997 Nuclear Science Symp
27. M. Moszynski, Nucl. Instr. and Meth in Phys. Res. A 350 (1994) 226 – 234
28. Technical documentation, Organic Scintillation Materials, Saint-Gobain (2001 – 15) http://www.crystals.saint-gobain.com/uploadedFiles/SG-Crystals/Documents/SGC%20Organics%20Brochure.pdf
29. Technical documentation, NaI(Tl) scintillation material, Saint-Gobain (2005 – 14) http://www.crystals.saint-gobain.com/uploadedFiles/SG-Crystals/Documents/NaI(Tl)%20Data%20Sheet.pdf
30. B. Sabbah, Nucl. Instr. and Meth, 58, (1968) 102
31. M. Flaska, Nucl. Instr. and Meth in Phys. Res. A 577 (2007) 654 – 663
32. A. Lintereur, Technical report, PNNL-21609 (March 2012)
33. R. Aryaeinejad, IEEE Nuclear Science Symposium Conference Record (Oct. 2005) 500 – 505
34. E. J. Axton and A. G. Bardell, Metrologia, Springer-Verlag 21, 59-74 (1985)
35. K. Nakamura, Nucl. Instr. and Meth in Phys. Res. A 623 (2010) 276 – 278
36. D. Reilly, N. Ensslin, H. Smith Jr., S. Kreiner, Passive non destructive assay of nuclear materials, Los Alamos, 1991, T.W. Crane and M.P. Baker, Neutron detectors 379 – 406
37. W.E. Spicer, A. Herrera-Gomez, Modern theory and applications of photocathodes, International Symposium on Optics, Imaging and Instrumentation, San Diego, USA (1993)

Acknowledgements

Firstly, I would like to acknowledge my supervisor Heikki Penttilä who contributed a big patience, hours of discussions and essential advices. Next I would like to thank Jaakko Julin for generous providing the data acquisition system. Also I would like to acknowledge the participation of my friend, Daniil Chapovskiy who helped me with the program code and with studying Python. I would like to thank a technical support from Raimo Seppälä and Mechanical and Electrical Workshops. Additional thanks to CEA France for the proposed unique sample of the plastic scintillator.

I would also like to acknowledge Professor Ari Jokinen for the opportunity to join the IGISOL group and possibility to conduct my master's research in IGISOL.

Individually I would like to thank my wife Kateryna Poleshchuk for her support and assistance in the experiment.

Finally, I would like to thank my parents Natalia and Pitter Poleshchuk for all the support and love they have given me.

Appendix 1 Calibration of voltage channels of digitizer Caen N6751

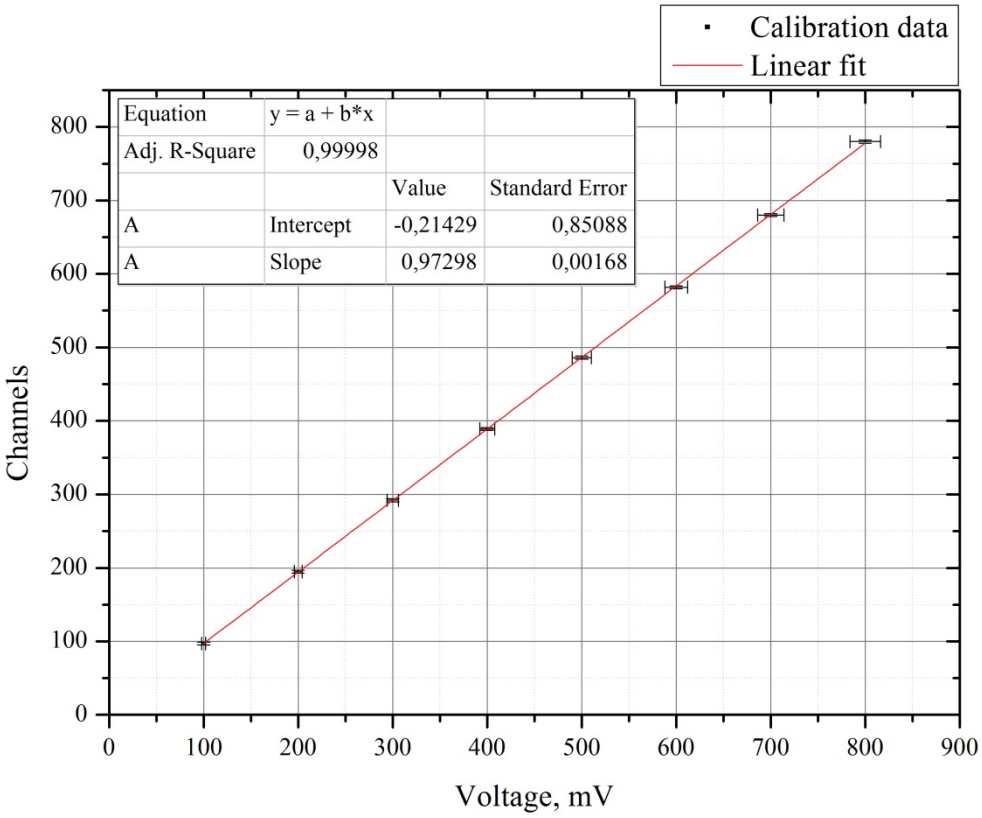

Fig. A1.1 Channels as a function of voltage.

Calibration of voltage channels of Caen N6751 digitizer was a necessary step in light yield determination, where channel – voltage conversion coefficient is required.

For calibration was used square pulses generated by oscilloscope Agilent Technologies DSO-X 3104A.Calibration was made in range 100 – 800 mV with step 100 mV. Amplitude accuracy declared by manufacturer is 2% at frequency 1 kHz.

The obtained data was fitted with linear equation. Dependence between channels and voltage is reflected in the next equation:

$$Ch_V = 0{,}973 \cdot V - 0{,}214 \quad \text{(A1.1)}$$

Appendix 2 Data analyzing code for realization of n-γ PSD technique

The program code was written in Python 2.7.10 using NumPy 1.8.1 and Matplot 1.3.1 modules. This code was optimized for data obtained from the data acquisition system described above. A sample of the data that was used for data analyzing is present in Table A2.1.

Table A2.1. Typical data structure that was used for data recording.

#File opened at UNIX time 1435418736.696	
BEGIN_EVENT	
Channel=3	
MChannel=2	
EventNumber=1	
Timestamp=21268096	10 lines
NumberOfValues=0	
NumberofWaveforms=1	
END_OF_HEADERS	
BEGIN_WAVEFORM	1st pulse
Waveform0=602	
815	
816	602 lines
…	
…	
815	
END_OF_WAVEFORM	2 lines
END_OF_EVENT	
BEGIN_EVENT	
Channel=3	
MChannel=2	
EventNumber=1	
Timestamp=21269104	
NumberOfValues=0	
NumberofWaveforms=1	
END_OF_HEADERS	
BEGIN_WAVEFORM	2nd pulse
Waveform0=602	
815	
816	
…	
…	
815	
END_OF_WAVEFORM	
END_OF_EVENT	
BEGIN_EVENT	
…	…
END_OF_EVENT	
BEGIN_EVENT	
…	nth pulse
END_OF_EVENT	

```
__author__ = 'Oleksii Poleshchuk'
from datetime import datetime
import numpy as np
import matplotlib.pyplot as plt
from matplotlib.patches import Polygon
import Tkinter as Tk
import tkFileDialog

print 'Program started at', datetime.now()

# Opening file with file dialog
root = Tk.Tk()
root.withdraw()
initial_file = tkFileDialog.askopenfile()

# Set of variables which contain information about initial file and settings
for data analysing.
# Some of these variables will be used to create a file name of the output
files and some for light yield calculation
file_name = raw_input('Write the name of the .evnt file: ')
source = raw_input('What was the source? ')
bias = raw_input('What was the bias? ')
cust_set = raw_input('If you would you like to use CUSTOM PARAMETERS for
LIGHT YIELD calculation such as:\n'
                     'scintillator type, a PMT gain, quantum efficiency of
the PMT, Compton pulse maximum,\n'
                     'or Compton edge energy, PRESS (y), if you would like to
use DEFAULT PARAMETERS PRESS (n): ')
if cust_set == 'y':
    scintillator = raw_input('What scintillator did you use?')
    gain = float(raw_input('Write the gain of the PMT: '))
    quantum_efficiency = float(raw_input('Write the quantum efficiency of the
PMT: '))
    max_of_compton_pulse = int(raw_input('Write the maximal voltage channel
of the pulse which correspond to the '
                                         'Compton edge: '))
    compton_edge_energy = float(raw_input('Write the Compton edge energy: '))
else:
    scintillator_check = raw_input('Did you use any type of scintillators?
(y/n) ')
    # Detector and radioactive source parameters:
    if scintillator_check == 'y':
        scintillator = raw_input('If you have used the Plastic scintillator
press (p),\n'
                                 'if you have used BC-501A scintillator press
(l),\n'
                                 'if you have used some other type of
scintillators press (any other letter): ')
        if scintillator == 'p':
            scintillator = 'Plastic scint.'
            if bias == '-1300V':
                gain = 54274.85904
                quantum_efficiency = 0.22
                if source == 'Na-22' or source == 'Na22':
                    max_of_compton_pulse = 76
                    compton_edge_energy = 1061.66
                elif source == 'Co-60' or source == 'Co60':
                    max_of_compton_pulse = 74
                    compton_edge_energy = 1040.8
                elif source == 'Cs-137' or source == 'Cs137':
                    max_of_compton_pulse = 32
                    compton_edge_energy = 477.334
                else:
```

```
                max_of_compton_pulse = 0
                compton_edge_energy = 1
            elif bias == '-1400V':
                gain = 112914.63311
                quantum_efficiency = 0.22
                if source == 'Na-22' or source == 'Na22':
                    max_of_compton_pulse = 163
                    compton_edge_energy = 1061.66
                elif source == 'Co-60' or source == 'Co60':
                    max_of_compton_pulse = 158
                    compton_edge_energy = 1040.8
                elif source == 'Cs-137' or source == 'Cs137':
                    max_of_compton_pulse = 68
                    compton_edge_energy = 477.334
                else:
                    max_of_compton_pulse = 0
                    compton_edge_energy = 0
            elif bias == '-1500V':
                gain = 222086.62162
                quantum_efficiency = 0.22
                if source == 'Na-22' or source == 'Na22':
                    max_of_compton_pulse = 320
                    compton_edge_energy = 1061.66
                elif source == 'Co-60' or source == 'Co60':
                    max_of_compton_pulse = 308
                    compton_edge_energy = 1040.8
                elif source == 'Cs-137' or source == 'Cs137':
                    max_of_compton_pulse = 138
                    compton_edge_energy = 477.334
                else:
                    max_of_compton_pulse = 0
                    compton_edge_energy = 1
            else:
                gain = 0
                quantum_efficiency = 0
                max_of_compton_pulse = 0
                compton_edge_energy = 1
        elif scintillator == 'l':
            scintillator = 'BC-501A'
            if bias == '-1300V':
                gain = 54274.85904
                quantum_efficiency = 0.28
                if source == 'Na-22' or source == 'Na22':
                    max_of_compton_pulse = 65
                    compton_edge_energy = 1061.66
                elif source == 'Co-60' or source == 'Co60':
                    max_of_compton_pulse = 63
                    compton_edge_energy = 1040.8
                elif source == 'Cs-137' or source == 'Cs137':
                    max_of_compton_pulse = 36
                    compton_edge_energy = 477.334
                else:
                    max_of_compton_pulse = 0
                    compton_edge_energy = 1
            elif bias == '-1400V':
                gain = 112914.63311
                quantum_efficiency = 0.28
                if source == 'Na-22' or source == 'Na22':
                    max_of_compton_pulse = 132
                    compton_edge_energy = 1061.66
                elif source == 'Co-60' or source == 'Co60':
                    max_of_compton_pulse = 129
                    compton_edge_energy = 1040.8
```

```
                elif source == 'Cs-137' or source == 'Cs137':
                    max_of_compton_pulse = 71
                    compton_edge_energy = 477.334
                else:
                    max_of_compton_pulse = 0
                    compton_edge_energy = 1
            elif bias == '-1500V':
                gain = 222086.62162
                quantum_efficiency = 0.28
                if source == 'Na-22' or source == 'Na22':
                    max_of_compton_pulse = 265
                    compton_edge_energy = 1061.66
                elif source == 'Co-60' or source == 'Co60':
                    max_of_compton_pulse = 260
                    compton_edge_energy = 1040.8
                elif source == 'Cs-137' or source == 'Cs137':
                    max_of_compton_pulse = 139
                    compton_edge_energy = 477.334
                else:
                    max_of_compton_pulse = 0
                    compton_edge_energy = 1
            else:
                gain = 0
                quantum_efficiency = 0
                max_of_compton_pulse = 0
                compton_edge_energy = 1
        else:
            scintillator = 'Unknown type of scint.'
            energy_coefficient_a = 0
            energy_coefficient_b = 0
            gain = 0
            quantum_efficiency = 0
            max_of_compton_pulse = 0
            compton_edge_energy = 1
    else:
        scintillator = ''
        gain = 0
        quantum_efficiency = 0
        max_of_compton_pulse = 0
        compton_edge_energy = 1

# The first and the last number of events which would be processed
first_event = int(raw_input('Write the number of the pulse from which(not
including) data analysing will star: '))
number_of_event = int(raw_input('How many pulses you would like to analyse?
'))
last_event = first_event + number_of_event

# Positions of tail and total bounds of a pulse could be set here:
cust_set_2 = raw_input('If you would you like to use CUSTOM PARAMETERS for
PSD such as:\n'
                       'position of tail integral of a pulse and position of
total integral, PRESS (y)\n'
                       'if you would like to use DEFAULT PARAMETERS PRESS
(n): ')
if cust_set_2 == 'y':
    tail_start_items = int(raw_input('Tail start (max+b): b='))
    pulse_end_items = int(raw_input('Pulse end (max+c): c='))
    pulse_start_items = int(raw_input('Pulse start (max-a): a='))
    if pulse_start_items > 0:
        pulse_start_items = -pulse_start_items
else:
    tail_start_items = 10
```

```
    pulse_end_items = 170
    pulse_start_items = -20


# Function which takes variable and determines is this variable integer or
not
def check_for_int(s):
    try:
        int(s)
        return True
    except ValueError:
        return False

# Calculation starts below
print 'Calculation starts at', datetime.now()

counter = 0
data_counter = 0
baseline_sum = 0
pure_pulse_counter = 0
appended_pure_pulse_counter = 0
pulse = []
pure_pulses = []
baseline = []
for item in initial_file:
    data_counter += 1
    if check_for_int(item[0]) and data_counter > first_event:
        counter += 1
        data_point = int(item.rstrip())
        pulse.append(data_point)
        if counter < 21:
            baseline_sum += data_point
    elif counter > 0 and check_for_int(item[0]) is False:
        pure_pulse_counter += 1
        if pure_pulse_counter > first_event:
            appended_pure_pulse_counter += 1
            pure_pulses.append(pulse)
            baseline.append(baseline_sum/20)
        if pure_pulse_counter == last_event:
            counter = 0
            pulse = []
            baseline_sum = 0
            break
        counter = 0
        pulse = []
        baseline_sum = 0
initial_file.close()

number_of_pulses = len(pure_pulses)
pulse_length = len(pure_pulses[0])

print number_of_pulses, 'pulses have been converted into a list'

print 'File has been converted into a list at', datetime.now()

# Creating two lists. One list will contain time and other list will contain
time channels.
time = []
t_channels = []
for item in xrange(pulse_length):
    time.append(((item + 1) * 1.0) / 2)
    t_channels.append(item+1)
```

```
# Flip vertical: negative pulse -> positive pulse
positive_pulse = []
positive_pulses = []
for item in xrange(number_of_pulses):
    for i in pure_pulses[item]:
        positive_pulse.append(baseline[item] - i)
    positive_pulses.append(positive_pulse)
    positive_pulse = []

print 'Pulses have been flipped at', datetime.now()

# Finding maximal voltage channel in all pulses
positive_pulses_max = []
for item in xrange(number_of_pulses):
    positive_pulses_max.append(max(positive_pulses[item]))

# Binning the list which contains all maximal values
max_sorted = []
v_channels_y = [0] * (max(positive_pulses_max) + 1)
for item in xrange(number_of_pulses):
    if positive_pulses_max[item] not in max_sorted:
        max_sorted.append(positive_pulses_max[item])
        v_channels_y[positive_pulses_max[item]] = 1
    else:
        v_channels_y[positive_pulses_max[item]] += 1
v_channels_x = range(len(v_channels_y))

print 'Voltage channels have been binned at', datetime.now()

# Writing the binned data into a file
energy_file = open('%s_%s_%s_%s_counts(v_channels).txt' % (file_name, source,
number_of_pulses, bias), 'w')
energy_file.write('channel, counts\n')
v_channels_file = open('%s_%s_%s_%s_v_channels.txt' % (file_name, source,
number_of_pulses, bias), 'w')
for item in xrange(len(v_channels_y)):
    energy_file.write('%s, %s\n' % (v_channels_x[item], v_channels_y[item]))
    v_channels_file.write('%s\n' % (v_channels_y[item]))
energy_file.close()
v_channels_file.close()

print 'Voltage channels have been wrote to a file at', datetime.now()

# Pulse shape discrimination is here. Calculating tail and total integrals of
pulses.
pulse_integral_list = []
tail_integral_list = []
tail_to_total_ratio_list = []
# Iteration over highest point of each pulse.
for item in positive_pulses:
    # Looking for the highest point of each pulse and its index in the list
    pos_of_max = item.index(max(item))
    # Defying the bounds of the total integral
    pulse_start = pos_of_max + pulse_start_items
    pulse_end = pos_of_max + pulse_end_items
    # Integration over all elements which are placed between the bounds we
defined above
    pulse_integral = sum(item[pulse_start:pulse_end + 1])
    pulse_integral_list.append(pulse_integral)
    # Defying the bounds of the tail integral (lower bound remains the same
as above)
    tail_start = pos_of_max + tail_start_items
    # Integration over all elements which are placed between the bounds we
```

```
defined above
    tail_integral = sum(item[tail_start:pulse_end + 1])
    tail_integral_list.append(tail_integral)
    # Calculation of the ratio (tail integral)/(total integral)
    if pulse_integral != 0:
        tail_to_total_ratio_list.append(round((tail_integral * 1.0) /
pulse_integral, 4))
    else:
        tail_to_total_ratio_list.append(0)

print 'Pulse shape discrimination has been done at', datetime.now()

# This part of the code calculates light yield of the pulses, which
correspond to the Compton edge.
light_yield_file = open('%s_%s_%s_%s_light_yield.txt' % (file_name, source,
number_of_pulses, bias), 'w')
light_yield_file.write('Number of photons in the pulse, Light yield
(photons/keV)\n')
anode_electrons_of_compton_pulse = []
photo_electrons_of_compton_pulse = []
scintillation_photons = []
light_yield_list = []
# Iteration over highest point of each pulse.
for item in xrange(len(positive_pulses_max)):
    # The next statement checks if a pulse highest point corresponds to the
highest point of the Compton pulse.
    # If this statement True the code will perform the calculation of light
yield.
    if positive_pulses_max[item] == max_of_compton_pulse:
        # To calculate amount of charge in one pulse was used next equation:
        # charge = 2*(sum(voltage_channel(ch))*voltage-
channel_coefficient(V/ch)*sample_rate(s))/impedance(Ohm)
        charge = 2*pulse_integral_list[item]*10**(-3)*0.973*0.5*10**(-9)/50
        # At the next step the collected charge was converted into amount of
anode electrons
        anode_electrons = charge/(1.6*10**-19)
        anode_electrons_of_compton_pulse.append(anode_electrons)
        # Here the anode electrons was converted into cathode electrons
        photo_electrons = anode_electrons/gain
        photo_electrons_of_compton_pulse.append(photo_electrons)
        # Number of photons emitted from scintillator was determined by
dividing cathode electrons by quantum efficiency
        photons = photo_electrons/quantum_efficiency
        scintillation_photons.append(photons)
        # To find the light yield, the number of photons was divided by
energy which correspond to this pulse
        light_yield = photons/compton_edge_energy
        light_yield_list.append(light_yield)
        light_yield_file.write('%s, %s\n' % (photons, light_yield))
light_yield_file.close()

print 'Light yield has been calculated and wrote to the file at',
datetime.now()

# Plots start below:
# Fig.1 An anode pulse with integration limits
fig1 = plt.figure()
ax1 = fig1.add_subplot(111)
the_displayed_pulse = positive_pulses[500]
ax1.plot(t_channels, the_displayed_pulse, label='%s, %s, %s' % (file_name,
source, bias))
plt.xlabel('Time', fontsize=15)
plt.ylabel('Amplitude', fontsize=15)
```

```
plt.xlim([(the_displayed_pulse.index(max(the_displayed_pulse)) - 40),
          (the_displayed_pulse.index(max(the_displayed_pulse)) + 220)])
# Make the shaded regions
a = (the_displayed_pulse.index(max(the_displayed_pulse)) + tail_start_items)
b = (the_displayed_pulse.index(max(the_displayed_pulse)) + pulse_end_items)
c = (the_displayed_pulse.index(max(the_displayed_pulse)) + pulse_start_items)
tail1x = np.linspace(a, b, num=(b-a+1))
tail1y = the_displayed_pulse[a-1:b]
total1x = np.linspace(c, b, num=(b-c+1))
total1y = the_displayed_pulse[c-1:b]
tail1 = [(a, 0)] + list(zip(tail1x, tail1y)) + [(b, 0)]
tail1area = Polygon(tail1, facecolor='0.6', edgecolor='y', hatch='/',
alpha=0.5,
                    label='Tail Integral: from b to c')
total1 = [(c, 0)] + list(zip(total1x, total1y)) + [(b, 0)]
total1area = Polygon(total1, facecolor='0.8', edgecolor='y', hatch='\\',
                     label='Total Integral: from a to c')
ax1.add_patch(total1area)
ax1.add_patch(tail1area)
ax1.set_xticks((a, b, c,
the_displayed_pulse.index(max(the_displayed_pulse))+1))
ax1.set_xticklabels(('$b$', '$c$', '$a$', '$m$'))
plt.ylim(-5, max(the_displayed_pulse) + 10)
ax1.plot([the_displayed_pulse.index(max(the_displayed_pulse))+1,
          the_displayed_pulse.index(max(the_displayed_pulse))+1], [0,
max(the_displayed_pulse)], 'g-.')
plt.xticks(fontsize=15)
plt.yticks(fontsize=15)
ax1.legend()
fig1.savefig('%s_%s_%s_%s_volt(time).png' % (file_name, source,
str(number_of_pulses), bias), dpi=300)

print '1st graph has been plotted at', datetime.now()

# Fig.2 Energy spectra
fig2 = plt.figure()
ax2 = fig2.add_subplot(111)
ax2.plot(v_channels_x, v_channels_y, 'b-', label='Total energy spectra')
plt.xlabel('Channels', fontsize=15)
plt.ylabel('Counts', fontsize=15)
ax2.grid()
plt.xticks(fontsize=15)
plt.yticks(fontsize=15)
plt.xlim(0, max(v_channels_x)+10)
plt.ylim(0, max(v_channels_y)+10)
ax2.legend()
fig2.savefig('%s_%s_%s_%s_counts(v_channels).png' % (file_name, source,
number_of_pulses, bias), dpi=300)

print '2nd graph has been plotted at', datetime.now()

# Fig.3 2D Histogram integral of Tail as function of integral of Total
fig3 = plt.figure()
fig3.add_subplot(111)
plt.suptitle('%s, %s, %s, %s' % (scintillator, source, number_of_pulses,
bias), fontsize=14)
plt.hist2d(pulse_integral_list, tail_integral_list, (1200, 1200), cmin=1,
cmap='gnuplot')
cb = plt.colorbar()
cb.set_label('Counts')
plt.xlabel('Total integral, Arbitrary Units', fontsize=15)
plt.ylabel('Tail integral, Arbitrary Units', fontsize=15)
plt.xticks(fontsize=15)
```

```
plt.yticks(fontsize=15)
plt.grid()
plt.ylim(0, 3000)
plt.xlim(0, 10000)
fig3.savefig('%s_%s_%s_%s_Tail_integral(Total_integral)_histogram_2D.png'
             % (file_name, source, number_of_pulses, bias), dpi=300)

print '3rd graph has been plotted at', datetime.now()

# Fig.4 Histogram of Tail to Total ratios
fig4 = plt.figure()
fig4.add_subplot(111)
plt.suptitle('%s, %s, %s, %s' % (scintillator, source, number_of_pulses,
bias), fontsize=14)
# the histogram of the data
bin_width = 0.01
bin_array = np.arange(0, max(tail_to_total_ratio_list) + bin_width,
bin_width)
plt.hist(tail_to_total_ratio_list, bins=bin_array, facecolor='green',
alpha=0.5,
         label='Tail Integral: max+%s / max+%s \nTotal Integral: max%s /
max+%s'
               % (tail_start_items, pulse_end_items, pulse_start_items,
pulse_end_items))
plt.xlabel('Ratio of tail-to-total integrals', fontsize=15)
plt.ylabel('Occurrence', fontsize=15)
plt.xticks(fontsize=15)
plt.yticks(fontsize=15)
plt.xlim(0, 1)
plt.legend()
fig4.savefig('%s_%s_%s_%s_Tail_to_Total_Ratio_histogram.png' % (file_name,
source, number_of_pulses, bias), dpi=300)

print '4th graph has been plotted at', datetime.now()
print 'Last calculation has been done at', datetime.now()
```